Journal of Magnetic Resonance 207 (2010) 176–189

Contents lists available at ScienceDirect

Journal of Magnetic Resonance

journal homepage: www.elsevier.com/locate/jmr

Perspectives in Magnetic Resonance

Theoretical aspects of dynamic nuclear polarization in the solid state – The solid effect

Yonatan Hovav, Akiva Feintuch, Shimon Vega *

Department of Chemical Physics, Weizmann Institute of Science, Rehovot, Israel

ARTICLE INFO

Article history:
Received 15 September 2010
Revised 27 October 2010

Keywords:
Dynamic nuclear polarization
Solid effect

ABSTRACT

Dynamic nuclear polarization has gained high popularity in recent years, due to advances in the experimental aspects of this methodology for increasing the NMR and MRI signals of relevant chemical and biological compounds. The DNP mechanism relies on the microwave (MW) irradiation induced polarization transfer from unpaired electrons to the nuclei in a sample. In this publication we present nuclear polarization enhancements of model systems in the solid state at high magnetic fields. These results were obtained by numerical calculations based on the spin density operator formalism. Here we restrict ourselves to samples with low electron concentrations, where the dipolar electron–electron interactions can be ignored. Thus the DNP enhancement of the polarizations of the nuclei close to the electrons is described by the Solid Effect mechanism. Our numerical results demonstrate the dependence of the polarization enhancement on the MW irradiation power and frequency, the hyperfine and nuclear dipole–dipole spin interactions, and the relaxation parameters of the system. The largest spin system considered in this study contains one electron and eight nuclei. In particular, we discuss the influence of the nuclear concentration and relaxation on the polarization of the core nuclei, which are coupled to an electron, and are responsible for the transfer of polarization to the bulk nuclei in the sample via spin diffusion.

1. Introduction

Dynamic nuclear polarization (DNP) is a method to enhance NMR signals by transferring spin polarization from paramagnetic ions or single unpaired electrons to their neighboring nuclei. Although DNP has been known to practitioners of magnetic resonance for almost half-a-century, in the last one and half decades the interest in this technique has increased significantly, mainly due to recently proposed potential applications to solid state NMR, NMR of biological systems and clinical MRI [1–5]. One of the main goals of current research in DNP is optimization of the technique so that one can achieve the largest nuclear polarization enhancement in the shortest time for different experimental conditions. This optimization can gain significantly from better theoretical understanding of the physical mechanisms involved in the process.

The DNP phenomena, was predicted by Overhauser in 1953 [6] and demonstrated by Carver and Slichter not long after [7]. Overhauser proposed that MW saturation of the "allowed" single quantum (SQ) EPR transitions of a conduction electron coupled to a nuclear spin in a metal-type sample would lead to polarization transfer from the electron spin to the nuclear spin. Subsequently this experiment was repeated on liquid solutions containing nuclear and electron spins [8,9]. The enhancement in these cases results from the difference between the zero quantum (ZQ) and double quantum (DQ) relaxation rates caused by field fluctuations originating from the motion of the electrons. A detailed description of the Overhauser effect can be found in the reviews of Hausser et al. and Mueller-Warmuth et al. [10,11].

Following these experiments Jeffries proposed in 1957 [12] that one can transfer polarization from the electron to the nucleus in a hyperfine coupled electron–nucleus pair by irradiating at the ZQ and DQ "forbidden" EPR transitions. As he describes it, the hyperfine coupling can result in some mixing between the Zeeman nuclear manifolds "allowing" these transitions. This mechanism was expected to be efficient for paramagnetic substances in the solid state. The theoretical foundations for what is known today as the "Solid Effect" (SE) were further developed and demonstrated experimentally by Abragam, Jeffries and others [13–17]. The theoretical approach was phenomenological by introducing rate equations that describe the effects of the microwave irradiation and the different relaxation mechanisms on the bulk polarization of the system. These models were used for qualitative predictions of the dependence of the SE enhancement

* Corresponding author. Fax: +972 8 934 4123.
E-mail address: shimon.vega@weizmann.ac.il (S. Vega).

1090-7807/$ - see front matter © 2010 Elsevier Inc. All rights reserved.
doi:10.1016/j.jmr.2010.10.016

on the microwave power and irradiation frequency and on the relaxation parameters [18–20]. The SE theory predicts that DQ and ZQ irradiations result in positive and negative enhancements of the NMR signals, respectively. A clear experimental signature of this mechanism is that, at least in the case when the ZQ and DQ transitions are well resolved, the difference in irradiation frequency of the positive and negative enhancement peaks is twice the nuclear Larmor frequency.

In 1964 Abragam and Borghini [21] reformulated the SE mechanism in terms of spin temperature theory, previously developed by Redfield [22], Solomon [23] and Provotorov [24]. In this framework the SE is described as cooling of the nuclear spin bath by the irradiation on the forbidden transitions. Spin temperature theory predicted however an additional effect which originates from the combined cooling of the electron spin–spin interaction bath and the cooling of the nuclear spin bath by excitation of the DQ or ZQ transitions. The irradiation frequencies for which this process will lead to the best positive or negative enhancement depend on the strength of the electron spin–spin interactions and are different from those of the SE. As a result when this effect dominates the DNP enhancement process the frequency difference between the positive and negative peaks in the DNP spectrum is smaller than twice the nuclear Larmor frequency. In 1967 Hwang and Hill showed, that when measuring proton enhancements in polystyrene doped with free radicals at low radical concentrations, one gets a SE type of frequency dependence. However, when the radical concentration is increased there is an additional enhancement of the positive and negative polarizations and their peak positions shift towards each other [25], just as predicted by Abragam and Borgini. Following these experimental results they proposed a theoretical model, based on previous work by Kessenikh and Manenkov [26,27], which takes into account the existence of separate electron spin packets in the case of an inhomogeneously broadened EPR line. The effect, which they called the Cross Effect (CE), results then from the electron dipole–dipole coupling between these spin packets, enabling transfer of spin populations between the packets combined with a flipping of nuclear spin states [28]. Based on their work, the term CE is now typically used to describe the process of MW-driven polarization transfer in a system with two interacting electron spins with Larmor frequencies separated by the nuclear Larmor frequency [29,30]. The process described by Abragam and Borghini was termed thermal mixing (TM) and is now used to describe systems with many interacting electrons coupled to nuclei as was described in a comprehensive review by Abragam and Goldman [19].

All mechanisms mentioned above describe the transfer of polarization from the electron spins to their nearby hyperfine coupled nuclear spins. To complete the picture it is necessary to realize that in typical DNP experiments the electron spin concentration is relatively low and the bulk nuclear polarization is achieved by an additional transfer of polarization from the nearby nuclei to the remote bulk nuclei *via* a spin diffusion process. The DNP process is therefore quite complex and many of the theoretical discussions of the different DNP mechanisms take only the first part of the transfer into account. For a qualitative understanding of the experimental results all different transfer aspects must be considered and an important example of such a study is the work of Wind and coworkers [20,31]. They were also the first to combine DNP with magic angle spinning (MAS). During the last 15 years Griffin and his coworkers have contributed much to the understanding, development, and applications of MAS–DNP as described in a recent review [32].

In the past years with the revival of interest in DNP one of the focuses has been on the enhancement of nuclear polarization during DNP experiments at high fields, where the early theories predicted a depletion of the enhancements. In the case of solution DNP at high fields, recent experimental results demonstrate that for high microwave powers one can achieve NMR signals that are higher than predicted theoretically [33–35]. For radicals mixed in frozen solutions, it has been shown that for systems in which the SE is the only DNP mechanism the enhancements are quite low [36,37]. However, for systems in which the CE and TM mechanisms dominate large nuclear signals are obtained at high fields [36,38]. Amplifying the microwave irradiation intensity increases the DNP yield even further. This was demonstrated by Griffin et al. after the introduction of a gyrotron as their microwave source, as reviewed in [32]. An additional improvement in enhancement was achieved by the introduction of bi-radicals as polarizers [39,32]. The increased electron spin dipole–dipole interaction in this case, due to the proximity of the two electron spins in the molecule, contribute to CE type processes. The search for the ideal polarizer (bi-radical, tri-radical, etc.) [38] is still ongoing and can definitely gain from a better understanding of the different DNP mechanisms.

In this and the following publication we intend to revisit the different solid-DNP mechanisms, by performing computer simulations of the nuclear polarization enhancement in model systems. The simulations are based on the spin density matrix formalism, using the full Liouville representation as well as approximate calculations of the quantum state populations using rate equations. This is different from the commonly used approach which as previously described is based on phenomenological rate equations for the spin polarization. Here we will restrict ourselves to the SE-DNP mechanism, while in the following publication we will discuss CE processes.

After the introduction of all relevant spin interactions in electron–nuclear spin systems, we will define the relaxation parameters that describe the spin–lattice and spin–spin mechanisms in these systems and discuss the effect of the microwave irradiation. We will then introduce the simulation procedures we have used and will apply these methods to follow the nuclear polarizations around a single electron, starting with a simple electron–nucleus two-spin system. We will then follow this process for three and nine-spin systems, and mention the complexity of larger spins systems when describing SE-DNP phenomena.

2. Theoretical methodology

2.1. The spin interactions and relaxation

Throughout this and the following paper we will concentrate on the spin dynamics of a system in the solid state, composed of N_e unpaired electrons ($S = 1/2$) and N_n equivalent nuclei ($I = 1/2$), in an external magnetic field. Taking the hyperfine and dipolar interactions between all $N = N_e + N_n$ spins into account, and assuming that the system experiences a continuous microwave (MW) irradiation, the spin Hamiltonian of this system in the MW rotating frame can be represented by [40]

$$H = H_Z + H_{hfi} + H_D + H_d + H_{MW} = H_0 + H_{MW}. \quad (1)$$

The first term H_Z corresponds to the off-resonance values of the electrons and the nuclear Zeeman interaction. The second term H_{hfi} represents the electron–nuclear hyperfine interaction (*hfi*), truncated with respect to the electron Zeeman interaction (i.e. keeping the pseudo-secular terms). The next two terms are the dipole–dipole interactions between the electrons a, $b = 1,\ldots,N_e$, represented by H_D, and between the nuclei $i,j = 1,\ldots,N_n$, represented by H_d. The last term, H_{MW}, represents a MW field applied in the x-direction, perpendicular to the external magnetic field. For simplicity, all spin interaction terms are combined in H_0, not including H_{MW}. The terms of H are given by:

$$H_Z = \sum_{a=1\ldots,N_e} \Delta\omega_a S_{z,a} - \omega_n \sum_{i=1,\ldots,N_n} I_{z,i}, \tag{2}$$

$$H_{hfi} = \sum_{\substack{a=1,\ldots,N_e \\ i=1,\ldots,N_n}} A_{z,ai} S_{z,a} I_{z,i} + \frac{1}{2}(A^{+}_{ai} S_{z,a} I^{+}_{i} + A^{-}_{ai} S_{z,a} I^{-}_{i}),$$

$$H_D = \sum_{a<b} D_{ab}(3S_{z,a}S_{z,b} - \bar{S}_a \cdot \bar{S}_b),$$

$$H_d = \sum_{i<j} d_{ij}(3I_{z,i}I_{z,j} - \bar{I}_i \cdot \bar{I}_j),$$

$$H_{MW} = \omega_1 \sum_{a=1,\ldots,N_e} S_{x,a}.$$

$\Delta\omega_a$ are the off-resonance values, defined by the difference between the electron Larmor frequencies $\omega_{e,a}$ and the MW frequency ω_{MW}, $\Delta\omega_a = \omega_{e,a} - \omega_{MW}$. $\omega_{e,a}$ is determined by the principal values and orientation of the $\bar{g}$-tensor of the electron a. The nuclear Larmor frequencies of all nuclei are assumed to be equal to ω_n, ignoring chemical shift differences. The *hfi* coefficients $A_{z,ai}$ and $A^{\pm}_{ai}$ are the secular and pseudo-secular parts of the electron–nuclear dipolar interaction, and $D_{a,b}$ and $d_{i,j}$ are the dipolar interaction coefficients between the electrons and the nuclei, respectively. These coefficients are proportional to $(r_{ai})^{-3}$, $(r_{ab})^{-3}$ and $(r_{ij})^{-3}$, respectively, and are anisotropic, depending on the polar angles defining the orientation of the vectors in the laboratory frame, $\bar{r}_{ai}, \bar{r}_{ab}$, and $\bar{r}_{ij}$, connecting the spins. Finally, ω_1 is the nutation frequency of the MW irradiation field. In the pure product states of the spins (where each individual spin is represented by its $|\alpha\rangle$ or $|\beta\rangle$ state) the pseudo-secular hyperfine terms, $A^{\pm}_{ai}$, and the flip–flop terms of H_D and H_d are off-diagonal. These terms are responsible for the DNP polarization transfer from the electrons to the nuclei in the system.

In addition to the static Hamiltonian we must include possible spin–lattice and spin–spin relaxation mechanisms in our description of the DNP signal enhancement. Here we will *not* derive explicit expressions for the T_1^{-1} and T_2^{-1} relaxation rates of our system but will only consider the type of interactions that are the sources of these rates. Thus we will introduce characteristic relaxation parameters that define the magnitudes of these rates. For a spin system defined by the spin Hamiltonian of Eq. (1), the thermal equilibrium state is defined by a density matrix ρ^{Λ}_{eq}, which is diagonal in the eigenstate representation of the Hamiltonian. We must therefore provide relaxation rates in this diagonalized frame. The diagonalization of H_0, of dimension $2^N \times 2^N$, can be represented by:

$$\Lambda_0 = D^{-1} H_0 D. \tag{3}$$

Applying the same diagonalization to the spin density operator $\rho(t)$ in the original product state representation gives:

$$\rho^{\Lambda}(t) = D^{-1}\rho(t)D. \tag{4}$$

The eigenstates of Λ_0 are written as: $|\lambda_k\rangle$, with $k = 1,\ldots,2^N$ and are linear combinations of the pure product states. The populations of the states are by definition equal to the diagonal elements:

$$p_k(t) = \langle\lambda_k|\rho^{\Lambda}(t)|\lambda_k\rangle. \tag{5}$$

In our calculations we will assign to each $|\lambda_k\rangle \rightarrow |\lambda_{k'}\rangle$ transition a spin–lattice relaxation rate, $T^{-1}_{1,kk'}$, affecting the difference between the populations $(p_k(t) - p_{k'}(t))$, and introduce spin–spin relaxation rates, $T^{-1}_{2,kk'}$, affecting the off-diagonal elements of the density matrix of the form $\langle\lambda_k|\rho^{\Lambda}(t)|\lambda_{k'}\rangle$.

The values of the single transition relaxation rates, $T^{-1}_{1,kk'}$, can be derived by assuming time fluctuating interactions proportional to some spin operator X_ξ that causes relaxation. The operator X_ξ can be linear, e.g. fluctuations in the coefficients of $2S_x$ and $2I_x$ which can be sources of $T^{-1}_{1,e}$ and $T^{-1}_{1,n}$, respectively, or bilinear, e.g. $4\sum_{a,i} A^{\pm\pm}_{ai} S^{\pm}_a I^{\pm}_i$, which can be sources of $T^{-1}_{1,DQ}$. We can generally assume that after diagonalization the effect of these fluctuations on each $|\lambda_k\rangle \rightarrow |\lambda_{k'}\rangle$ transition is proportional to the squares of matrix elements $|\langle\lambda_k|D^{-1}X_\xi D|\lambda_{k'}\rangle|^2$ [18]. Our approach in this paper is therefore to chose a set of $\left[T_1^{-1}\right]_\xi$ relaxation rates for the pure product state system which are in the order of the magnitude of experimentally known values (when available). Based on these rates we calculate the rates of the individual transitions in the diagonalized Λ_0 representation, using

$$T^{-1}_{1,kk'} = \sum_{\xi} |\langle\lambda_k|D^{-1}X_\xi D|\lambda_{k'}\rangle|^2 \left[T_1^{-1}\right]_\xi, \tag{6}$$

where we sum over all basic relaxation mechanisms.

When we apply the diagonalization matrix D on the interaction Hamiltonian H_0, we must do the same to H_{MW}, resulting in $\Lambda_{MW} = D^{-1}H_{MW}D$. The matrix elements of Λ_{MW}, which connect the eigenstates of Λ_0, can be considered as effective MW irradiation fields applied on specific transitions

$$\omega_{1,kk'} = 2\langle\lambda_k|D^{-1}H_{MW}D|\lambda_{k'}\rangle. \tag{7}$$

During the DNP experiments we are interested in monitoring the NMR free induction decay signals of the nuclei after a single 90° pulse. The initial intensity of these signals can be determined by calculating

$$S_i(t) = Tr(\rho^{\Lambda}(t)D^{-1}I_{z,i}D), \tag{8}$$

for each spin i prior to the application of the pulse at time t. In the diagonal representation these intensities are linear combinations of the diagonal and off-diagonal elements of $\rho^{\Lambda}(t)$. The contributions from these off-diagonal elements can become significant when they are large. Their magnitudes are mainly determined by the MW irradiation fields $\omega_{1,kk'}$ (note that Λ_0 is diagonal) and the relaxation rates $T^{-1}_{2,kk'}$. In addition they can exhibit oscillating time dependences induced by Λ_0. As long as these elements are small, we can neglect their contributions to $S_i(t)$ and can replace the initial signal intensities by polarizations, defined as:

$$P_i(t) = Tr([[\rho^{\Lambda}(t)]]D^{-1}I_{z,i}D), \tag{9}$$

where the operator $[[\rho^{\Lambda}(t)]]$ contains only the diagonal matrix elements of $\rho^{\Lambda}(t)$. These polarizations are thus only dependent on the populations of the $|\lambda_k\rangle$ states. As will be shown later, in the DNP experiments discussed here the off-diagonal elements of $\rho^{\Lambda}(t)$ during the MW irradiation can indeed be ignored and we will only consider the populations $P_i(t)$, even when we discuss NMR signals.

The result of the DNP process can be characterized in several ways. One option is to follow the polarization of the nuclei $P_i(t)$ as defined in Eq. (9). Another possibility, which is more relevant experimentally, is to define the enhancement factor as

$$\pi_{n;i} = P_i(t)/P_i(0), \tag{10}$$

where $P_i(0)$ are the thermal equilibrium polarizations

$$P_i(0) = Tr\left(\left[\left[\rho^{\Lambda}_{eq}\right]\right]D^{-1}I_{z,i}D\right). \tag{11}$$

For the theoretical description it is more convenient to compare the nuclear polarizations with the thermal equilibrium polarization of the electron,

$$P_a(0) = -Tr\left(\left[\left[\rho^{\Lambda}_{eq}\right]\right]D^{-1}S_{z,a}D\right), \tag{12}$$

defining an enhancement factor

$$\pi_{e;i}(t) = P_i(t)/P_a(0). \tag{13}$$

The advantage of this definition is that the denominator does not depend on the choice of the nucleus.

In summary, our spin system is thus defined by the interaction coefficients $A_{z,ai}$, $A^{\pm}_{ai}, D_{ab}$ and d_{ij} in Eq. (2), derived from the spatial

configuration of the system, and the relaxation rates $T^{-1}_{1/2,kk'}$. During cw DNP experiments the MW irradiation is defined by the parameters ω_1 and $\Delta\omega_a$. As will be shown, in order to describe the polarization enhancements, we must take all these parameters simultaneously into account.

In the forthcoming sections we will use Eq. (13) to evaluate the efficiency of a DNP experiment and follow these parameters for different spin systems as a function of the relaxation parameters and MW irradiation fields.

2.2. The core and bulk nuclei

It is customary to distinguish between "core" and "bulk" nuclear spins. The distinction between these two types depends on the relative strength of the hyperfine interactions with respect to the nuclear dipole–dipole interactions H_d. The diagonal terms of the *hfi* can truncate the off diagonal flip–flop terms of H_d and thereby reduce the polarization transfer efficiency between the nuclei. We will define the "core" nuclei as those that are coupled to one or more electrons *via* a hyperfine interaction that is strong enough to truncate significantly the dipolar flip–flop matrix elements with their neighboring nuclei. The rest or "bulk" nuclei are coupled *via* dipole–dipole interactions that are not or only partially quenched by the hyperfine interactions. The boundary between these two kinds of nuclei in a spin system is not well defined and depends on the condition one chooses for the hyperfine truncation efficiency.

Thus in order to make a clear distinction between core and bulk nuclei, and without introducing a third kind of "boundary" nuclei, we must define a set of conditions that determine which nuclei belong to the core. The question of defining this boundary also known as the "diffusion barrier" has been discussed in the context of spin diffusion and different definitions can be found as summarized recently [41]. We have chosen that a nucleus i belongs to our core when the magnitudes of the off-diagonal matrix elements $d_{ij}/2$, connecting states that differ in $\alpha_i\beta_j \leftrightarrow \beta_i\alpha_j$, are smaller than one fifth of the differences between their corresponding diagonal matrix elements. These differences are determined by the *hfi* matrix elements and we define therefore that the core nuclei satisfy:

$$5|d_{i,j}/2| < \frac{1}{2}\left(|A_{z,ai} - A_{z,aj}| + \frac{1}{8\omega_n}\left|\left(\left|A^{\pm}_{a,i}\right|^2 - \left|A^{\pm}_{a,j}\right|^2\right)\right|\right). \quad (14)$$

Here we take into account the shifts of the diagonal elements induced by the pseudo-secular terms of the *hfi* calculated by perturbation theory. Our condition for the core nuclei defined in Eq. (14) is of course somewhat arbitrary, but it provides insight into the size and shape of the core around, for example, a single electron. We do realize that the core and bulk nuclei at the core-bulk interface do not necessarily differ much in terms of their hyperfine and dipole–dipole interaction. In most NMR experiments on DNP enhanced signals we detect mainly bulk nuclei, while the DNP mechanisms enhance directly the polarization of the core nuclei. Thus, a necessary step in the enhancement of NMR signals is the spin diffusion process. Here we are mainly interested in the SE mechanism which enhances the core nuclei. We will leave the discussion of the spin diffusion (SD) process in multi-nuclear spin systems for later. The polarization transfer to the bulk nuclei during the DNP process *via* SD in a model system will be discussed in a future publication.

Before continuing our description of the DNP mechanisms, we first show an example of the configuration of the core around a single electron. In Fig. 1 two core configurations are shown: One for a system of protons located on a simple cubic lattice with an electron at the center of the lattice and a unit vector of 3.1 Å. The other of ^{13}C spins in a similar lattice with a unit vector of 10.4 Å. These

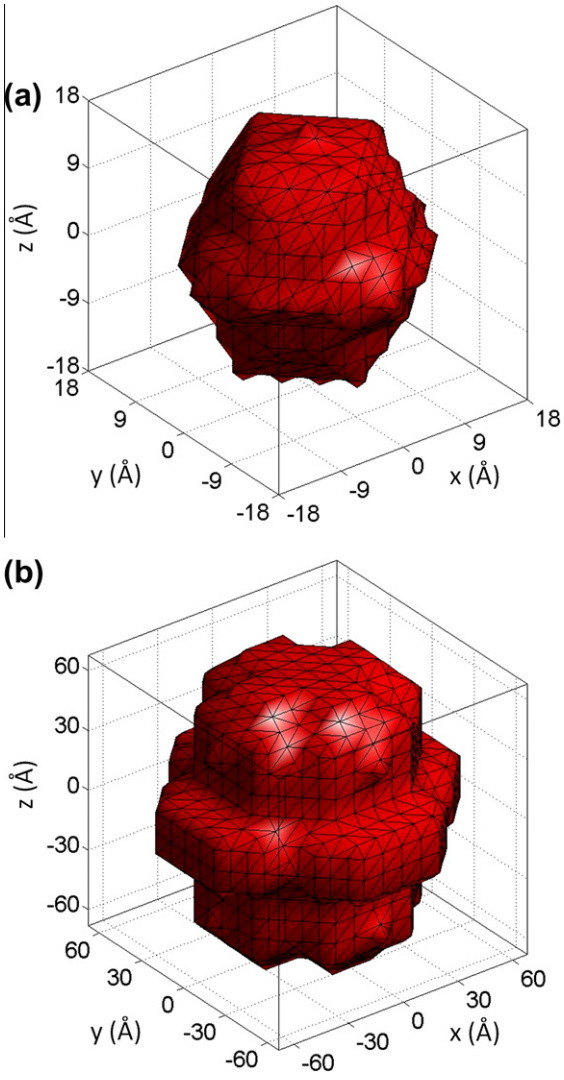

Fig. 1. Configurations of the core nuclei around a single electron, as defined in Eq. (14). These configurations were calculated assuming a simple cubic lattice of nuclei with a single electron at the center. In (a) the nuclei are all ^{1}H and the length of the lattice parameter is 3.1 Å and in (b) the nuclei are ^{13}C and the lattice parameter is 10.4 Å. The external magnetic field points in the z-direction.

distances correspond to a nuclear spin concentration of 55 M and 1.5 M, respectively. The volume of the core decreases with γ or with an increase of the concentration of the nuclear spins.

2.3. The EPR and NMR spectra

At this point it is important to discuss some general features of the EPR and NMR spectra of our spin systems. Although most of this discussion is well known, in particular to the EPR community, we will use it to introduce some concepts that will assist us in the rest of the paper. The frequency ranges of the two types of spectra are determined by the frequencies of the detectable transitions between the eigenstates of the Hamiltonian. Starting from a basis set of pure product states spanning H_0, we can group these states according to the sum of the z-components of the angular momenta of the electrons and nuclei, noted by M_e and M_n respectively. Each interaction term of H_0 in Eq. (2) has its own on- and off-diagonal matrix elements in this representation. The diagonal elements of H_Z determine the rotating frame Zeeman energies of the degenerate $\{|M_e, M_n 0\rangle\}$ manifolds of states. The diagonal elements of the

hfi and the dipolar interactions must be added to those energies and are proportional to $A_{z,ai}/4$, $D_{ab}/2$ and $d_{ij}/2$, respectively. The off-diagonal elements of the pseudo-secular *hfi* terms connect states with $\Delta M_n = \pm 1$, the nuclear *d*-interactions connect states with $\Delta M_n = 0$, and the electronic *D*-dipolar interactions with $\Delta M_e = 0$. Therefore, during diagonalization of H_0 the dipolar interactions mix states inside each $\{|M_e, M_n\rangle\}$ manifold, while the pseudo-secular *hfi* mixes states with $\Delta M_n = \pm 1$, and to a much lower extent with $|\Delta M_n| > 1$. As a result the mixed eigenstates can still be assigned by well defined M_e values, while the nuclear states are mixed. However, when $|A_{ai}^{+}| \ll \omega_n$ we can keep assigning the eigenstates of the whole system according to $\{|[M_e],\ [M_n^*]\rangle\}$, where the brackets indicate the state mixing by the dipolar interactions and the asterix the fact that there is a minor mixing of states with $\Delta M_n \neq 0$.

The observed spectra are determined by the values of matrix elements of S_a^+ and I_i^+ between eigenstates. The NMR spectrum appearing around ω_n, corresponds to the transition between states with $\Delta M_n = \pm 1$ and $\Delta M_e = 0$. Its spectral lines are (homogeneously) broadened due to the *d*-interactions and split by the *hfi*. The dipolar broadening can be up to tens of kHz for protons and the hyperfine splittings up to several MHz. These last splittings are in general not detectable in standard NMR experiments.

The EPR spectrum is composed of spectral lines with $\Delta M_e = \pm 1$. The nuclear selection rules for the EPR spectrum are mainly $\Delta M_n = 0$, but can also be equal to $\Delta M_n \neq 0$. The spectrum can therefore be subdivided into the main spectral band and the "forbidden" bands, respectively. The main band is of course inhomogeneously broadened by the off-resonance shifts $\Delta\omega_a$ and the diagonal *hfi* and *D*-coefficients and homogeneously broadened by the flip–flop terms of H_D. For small N_e values this band is composed of a set of isolated lines. The "forbidden" bands are removed from the $\Delta\omega_a$ positions in the main band by about $\pm\omega_n$ and in principle also by $\pm 2\omega_n$, etc. The contributions of the latter will be small and will be left out of our discussion. Thus we can distinguish between two forbidden frequency bands: the double quantum (DQ) spectrum with $\Delta M_e = \pm 1,\ \Delta M_n^* = \pm 1$ and the zero quantum (ZQ) spectrum with $\Delta M_e = \pm 1,\ \Delta M_n^* = \mp 1$. The positions of the DQ and ZQ spectra can overlap with the main band, depending on their width. Their spectral features are determined by all interactions and therefore these spectra have a similar width as the main EPR band but significantly lower amplitudes.

The EPR spectrum will of course become simple when the system contains a very small number of interacting electrons. For example, a spin system similar to that used in Fig. 1 has an EPR spectrum shown in Fig. 2. Here the frequencies of the DQ or ZQ transitions associated with each nucleus *i* are determined by evaluating the eigenvalues of $H_Z + H_{hfi}$, ignoring the pseudo-secular terms and the dipolar terms, and searching for transition frequencies between pairs of states that differ only in $\beta_e\beta_i \leftrightarrow \alpha_e\alpha_i$ or $\beta_e\alpha_i \leftrightarrow \alpha_e\beta_i$, respectively. The amplitudes of these transitions were set equal to $\left(|A_i^{\pm}|/2\omega_n\right)^2$. All transitions of all spins were broadened by a spin–spin relaxation rate $T_2^{-1} = 2 \times 10^5\ \mathrm{s}^{-1}$ and were added together. The two important factors determining the overall shape of the EPR spectrum are the gyromagnetic ratio of the nuclei, γ, and their concentration. The ratio γ will effect both ω_n and all *hfi* coefficients, while the concentration affects only the *hfi*. The positions of the centers of the ZQ/DQ transitions relative to the main EPR line depend only on γ and their intensities only on the concentration.

In many modern DNP studies the samples are amorphous glasses, containing radicals with randomly oriented *g*-tensors resulting in powder spectra. Experimentally, we are therefore observing spectra of electrons with different $\Delta\omega_a$ values which interact with each other, resulting in typical homogeneously and inhomogeneously broadened EPR powder spectra. In the present paper we will mainly consider spin systems that are composed of a single electron that is not interacting with neighboring electrons and that is surrounded by a collection of core nuclei. In the case, where powders or non-crystalline samples are considered, the spectra are a sum of individual spectra of non-interacting and randomly orientated electron-core systems. In our next publication on CE-DNP this restriction will be removed and electron–electron interactions will be taken into account.

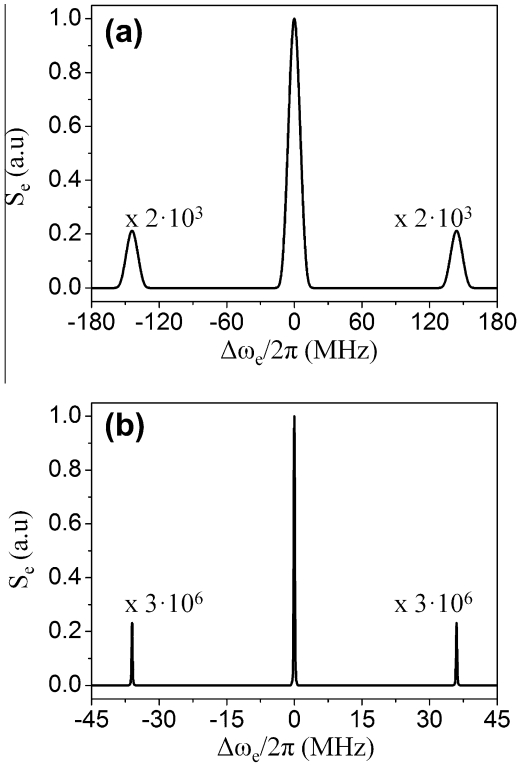

Fig. 2. The EPR spectra of the model $e{-}n_{N_n}$ systems used for Fig. 1 with (a) a cubic lattice of ^{1}H nuclei and (b) of ^{13}C nuclei. For the calculation all nuclei in a cube of $10 \times 10 \times 10$ spins around the electron were taken into account while the direction of the magnetic field was making an angle of 10° with the *z*-axis of the cube. The spectra were simulated using the secular terms of the *hfi*, $A_{zi}S_zI_{zi}$, and calculating the transition probabilities of the DQ and ZQ transitions corresponding to each nucleus according to $\left(|A_i^{\pm}|/2\omega_n\right)^2$. In the figure the ZQ and DQ spectra were multiplied by a factor of 2×10^3 and 3×10^6, respectively. The lines were convoluted using a Lorentzian line shape with a width of T_2^{-1}/π, where $T_2^{-1} = 2 \times 10^{-5}\ \mathrm{s}^{-1}$.

3. Methods of simulations

3.1. Calculations in Liouville space

In order to study the DNP mechanisms we will follow the time evolution of the spin density operator $\rho(t)$ of the spin system under investigation. This is influenced by the parameters of the interactions included in H_0, by H_{MW} and by the relaxation rates. These can all be combined in the Liouville superoperator [43] which determines the temporal evolution of $\rho(t)$. Before transferring the Hamiltonian to its superoperator form, we diagonalize H_0 as in Eq. (3), resulting in Λ_0 with eigenvalues λ_k and eigenstates $|\lambda_k\rangle$. Next the diagonalization matrix *D* is applied to the MW terms, resulting in $\Lambda_{MW} = D^{-1}H_{MW}D$, which remains non-diagonal. Then we transfer $\Lambda_0 + \Lambda_{MW}$ to its Liouville superoperator form, with elements $\langle\lambda_k, \lambda_{k'}|\Lambda_0 + \Lambda_{MW}|\lambda_{k''}, \lambda_{k'''}\rangle$, and try to solve the equation:

$$\frac{d\bar{\rho}^{\Lambda}(t)}{dt} = -(i(\widehat{\Lambda}_0 + \widehat{\Lambda}_{MW}) + \widehat{R})\bar{\rho}^{\Lambda}(t), \tag{15}$$

where $\bar{\rho}^{\Lambda}$ is a vector composed of the elements of the density matrix $\rho^{\Lambda}(t) = D^{-1}\rho(t)D$. $\widehat{R}$ is the relaxation superoperator composed

of all relaxation rates $T^{-1}_{1/2,kk'}$. The formal solution of the above rate equation for the time independent $\widehat{\Lambda}_0$, $\widehat{\Lambda}_{MW}$ and $\widehat{R}$ superoperators is

$$\bar{\rho}^{\Lambda}(t) = \widehat{U}(t)\bar{\rho}^{\Lambda}(0) \tag{16}$$
$$\widehat{U}(t) = \exp\{-(i(\widehat{\Lambda}_0 + \widehat{\Lambda}_{MW}) + \widehat{R})t\}.$$

The elements of the thermal equilibrium spin density vector, in the diagonalized frame, are given by:

$$p_k(0) = Z^{-1}\exp\{-(\lambda_k + \omega_{MW}M_{e,k})\hbar/k_BT\}, \tag{17}$$

where $M_{e,k}$ is the total z-component of the $|\lambda_k\rangle$ state and ω_{MW} is the MW irradiation frequency, determining the transformation operator to the rotating frame. Z is a normalizing partition function such that $Tr(\rho^{\Lambda}(0)) = 1$, k_B is the Boltzmann constant, and T is the temperature.

The $\widehat{R}$ supermatrix is constructed from individual spin–lattice and spin–spin relaxation rates $T^{-1}_{1,kk'}$ and $T^{-1}_{2,kk'}$ of all transitions $|\lambda_k\rangle \rightarrow |\lambda_{k'}\rangle$. The actual values of these rates will be discussed later. The matrix elements of $\widehat{R}$ are equal to a sum of single transition operators $\widehat{R}_{2,kk'}$ and $\widehat{R}_{1,kk'}$

$$\widehat{R} = \sum_{k<k'}\widehat{R}_{2,kk'} + \widehat{R}_{1,kk'} \tag{18}$$

with

$$\langle\lambda_k,\lambda_{k'}|\widehat{R}_{2,kk'}|\lambda_k,\lambda_{k'}\rangle = \langle\lambda_{k'},\lambda_k|\widehat{R}_{2,kk'}|\lambda_{k'},\lambda_k\rangle = \frac{1}{T_{2,kk'}} \tag{19}$$

and

$$\langle\lambda_k,\lambda_k|\widehat{R}_{1,kk'}|\lambda_k,\lambda_k\rangle = \frac{\varepsilon_{kk'}}{1+\varepsilon_{kk'}}\frac{1}{T_{1,kk'}} \tag{20}$$
$$\langle\lambda_k,\lambda_k|\widehat{R}_{1,kk'}|\lambda_{k'},\lambda_{k'}\rangle = -\frac{1}{1+\varepsilon_{kk'}}\frac{1}{T_{1,kk'}}$$
$$\langle\lambda_{k'},\lambda_{k'}|\widehat{R}_{1,kk'}|\lambda_{k'},\lambda_{k'}\rangle = \frac{1}{1+\varepsilon_{kk'}}\frac{1}{T_{1,kk'}}$$
$$\langle\lambda_{k'},\lambda_{k'}|\widehat{R}_{1,kk'}|\lambda_k,\lambda_k\rangle = -\frac{\varepsilon_{kk'}}{1+\varepsilon_{kk'}}\frac{1}{T_{1,kk'}},$$

with the Boltzmann factors

$$\varepsilon_{k,k'} = \exp\{(\lambda_k - \lambda_{k'})\hbar/k_bT\}. \tag{21}$$

The values of $T^{-1}_{1,kk'}$ were determined in two ways. In the case of an e–n spin system, we chose a single $T^{-1}_{1,e}$ value for all main EPR transitions, $T^{-1}_{1,DQ} = T^{-1}_{1,ZQ}$ values for the ZQ and DQ transitions and a nuclear $T^{-1}_{1,n}$ for the core nucleus (Fig. 3). In the e–n_2 and e–n_8 model systems, we begin with a choice of $T^{-1}_{1,e}$ and nuclear $T^{-1}_{1,i=1\ldots N_n}$ values in the pure product representation and calculate the values $T^{-1}_{1,kk'}$ in the diagonalized representation, assuming a source of relaxation as described in Section 2.1. For $T^{-1}_{2,kk'}$ we assign

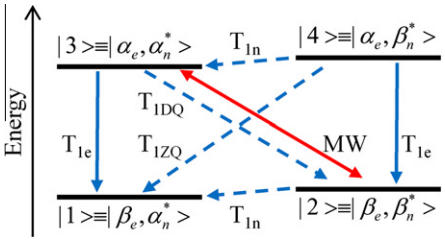

Fig. 3. Energy level diagram of a two-spin e–n system. The *'s indicate the small state mixing due to the pseudo-secular part of the *hfi* at high fields. The spin–lattice relaxation time of the electron, $T_{1,e}$, is indicated by the blue solid arrows, and those of the nucleus and the DQ and ZQ transitions, $T_{1,n}$ and $T_{1,DQ/ZQ}$, by blue dashed arrows. In addition, the *DQ* MW irradiation is indicated by the red double headed arrow. The electron Zeeman energies are scaled.

to all transitions with $\Delta M_e = 0$ a value $T^{-1}_{2,n}$, and to all EPR transitions, with $\Delta M_e = \pm 1$, a value $T^{-1}_{2,e}$. Overall, an effort was made to chose relaxation rates that are of the order of magnitudes found in actual experimental systems.

3.2. Calculations in Hilbert space

During the Liouville space calculations we must diagonalize the Liouville superoperator which is of size $4^N \times 4^N$ in a N-spin system. In practice these dimensions limit our ability to solve the Von-Neumann–Liouville equation numerically for large N values. In an upcoming publication we will show that in the case of SE-DNP we can derive coupled rate equations for the populations of the eigenstates of the spin interaction Hamiltonian, introducing a rate matrix of size $2^N \times 2^N$. The evolution of the spin polarizations in the system can then be calculated by diagonalization of the rate matrix. To derive the rate equations we must first diagonalize our Hamiltonian in Hilbert space, $\Lambda_0 = D^{-1}H_0D$ as previously described, resulting in eigenstates $|\lambda_k\rangle$ with $k = 1,\ldots,2^N$. In this representation the matrix elements of the density operator are $\langle\lambda_k|\rho^{\Lambda}|\lambda_{k'}\rangle$, where $\rho^{\Lambda}(t) = D^{-1}\rho(t)D$. Applying D to the MW Hamiltonian will result in off-diagonal matrix elements of magnitude $\omega_{1,kk'} = 2\langle\lambda_k|D^{-1}H_{MW}D|\lambda_{k'}\rangle$ that represent single transition effective MW irradiation fields. These effective MW fields have off-resonance values defined by $\Delta\omega_{kk'} = \langle\lambda_k|\Lambda_0|\lambda_k\rangle - \langle\lambda_{k'}|\Lambda_0|\lambda_{k'}\rangle$. The relaxation parameters introduced earlier are also defined as single transition relaxation rates $T^{-1}_{1,kk'}$ and $T^{-1}_{2,kk'}$. Each transition in the eigenstate manifold of the spin system is therefore characterized by its own MW, off-resonance and relaxation rates. We can now derive the dynamics of the whole spin system by simultaneously solving the Bloch equations for the populations, $\langle\lambda_k|\rho^{\Lambda}(t)|\lambda_k\rangle$, and coherences, $\langle\lambda_k|\rho^{\Lambda}(t)|\lambda_{k'}\rangle$, of each single transition. In the SE-DNP case, when $\omega_{1,kk'}, T^{-1}_{1,kk'} \ll T^{-1}_{2,kk'}$, the time evolutions of the population differences are (almost) independent of the coherences such that the latter can be neglected when $\langle\lambda_k|\rho^{\Lambda}(0)|\lambda_k\rangle \neq 0$ and $\langle\lambda_k|\rho^{\Lambda}(0)|\lambda_{k'}\rangle = 0$. Thus the calculations can be restricted to the populations only, and we can write a rate equation for the vector of all populations $\bar{p}^{\Lambda}(t)$ with elements $p^{\Lambda}_k(t) = \langle\lambda_k|\rho^{\Lambda}(t)|\lambda_k\rangle$:

$$\frac{d}{dt}\bar{p}^{\Lambda}(t) = -(R_{MW} + R_1)\bar{p}^{\Lambda}(t). \tag{22}$$

The $2^N \times 2^N$ rate matrix has two parts: the MW matrix $R_{MW} = \sum_{k<k'}R_{MW,kk'}$ is composed of a sum of $R_{MW,kk'}$, which have nonzero elements that are derived from the reduced Bloch equation population differences when $\omega_{1,kk'}, T^{-1}_{1,kk'} \ll T^{-1}_{2,kk'}$ for each k, k' pair:

$$\langle\lambda_k|R_{MW,kk'}|\lambda_k\rangle = \langle\lambda_{k'}|R_{MW,kk'}|\lambda_{k'}\rangle = \frac{(\omega_{1,kk'})^2T_{2,kk'}}{1+\Delta\omega_{kk'}T_{2,kk'}} \tag{23}$$
$$\langle\lambda_k|R_{MW,kk'}|\lambda_{k'}\rangle = \langle\lambda_{k'}|R_{MW,kk'}|\lambda_k\rangle = -\frac{(\omega_{1,kk'})^2T_{2,kk'}}{1+\Delta\omega_{kk'}T_{2,kk'}};$$

and the spin–lattice relaxation matrix $R_1 = \sum_{k<k'}R_{1,kk'}$, where the $R_{1,kk'}$ matrixes have nonzero elements derived using the expressions in Eq. (20):

$$\langle\lambda_k|R_{1,kk'}|\lambda_k\rangle = -\langle\lambda_{k'}|R_{1,kk'}|\lambda_k\rangle = \frac{\varepsilon_{kk'}}{1+\varepsilon_{kk'}}\frac{1}{T_{1,kk'}} \tag{24}$$
$$\langle\lambda_{k'}|R_{1,kk'}|\lambda_{k'}\rangle = -\langle\lambda_k|R_{1,kk'}|\lambda_{k'}\rangle = \frac{1}{1+\varepsilon_{kk'}}\frac{1}{T_{1,kk'}}.$$

The solution of Eq. (22) provides us with the time dependent populations from which we can evaluate the polarizations of the individual spins by calculating the dot-product

$$P_i(t) = \bar{p}^{\Lambda}(t)\cdot\overline{I_{z,i}}, \tag{25}$$

where $\overline{I_{z,i}}$ is a vector composed of all diagonal elements of $D^{-1}I_iD$.

4. The solid effect – theory and simulations

The SE -DNP mechanism is responsible for the polarization enhancement of nuclei surrounding a single electron. The Hamiltonian of such an electron coupled to N_c nuclei is defined by the off-resonance term $\Delta\omega_e S_z$, the nuclear Zeeman terms $\sum_i \omega_n I_{z,i}$, the electron–nuclear *hfi* terms $\sum_i \{A_{z,i} I_{z,i} + \frac{1}{2}(A_i^+ I_i^+ + A_i^- I_i^-)\} S_z$ and the nuclear dipole–dipole interaction terms $\sum_{i<j} d_{ij}(3I_{z,i}I_{z,j} - \bar{I}_i \cdot \bar{I}_j)$. Here we consider only spin systems with hyperfine interactions that are much smaller than the nuclear Zeeman interaction, $A_{zi},\ A_i^{\pm} \ll \omega_n$. In what follows we also limit ourselves to the polarization of (core) nuclei which are in proximity to the electron. The d_{ij} parameters of these nuclei are partially quenched by the *hfi*, but can become significant, in particular for core nuclei removed from the electron. We will begin our discussion with a two-spin *e*–*n* case and describe the basic nuclear SE enhancement mechanism. Then we will extend the system to three-spin *e*–n_2 and nine-spin *e*–n_8 systems, and we will end with some remarks concerning multi-nuclei core systems.

4.1. The e–n spin system

4.1.1. Ideal DNP polarization enhancement

The simplest system exhibiting the SE is a single electron coupled to a single nucleus. The spin Hamiltonian H_0 can be easily represented in the simple product states composed of $|M_e\rangle = |\alpha_e\rangle$, $|\beta_e\rangle$ and $|M_n\rangle = |\alpha_n\rangle$, $|\beta_n\rangle$. The only off-diagonal elements of the spin Hamiltonian of this system are the $A^{\pm}/4$ pseudo-secular terms between the states $|\alpha_e,\alpha_n\rangle$ and $|\alpha_e,\beta_n\rangle$ and between $|\beta_e,\alpha_n\rangle$ and $|\beta_e,\beta_n\rangle$. Diagonalization of H_0 is therefore straightforward (namely two 2×2 diagonalizations), resulting in [40]:

$$\begin{aligned}
|\lambda_1\rangle &= |\beta_e,\alpha_n^*\rangle = c^{\beta}|\beta_e,\alpha_n\rangle + s^{\beta}|\beta_e,\beta_n\rangle \\
|\lambda_2\rangle &= |\beta_e,\beta_n^*\rangle = -s^{\beta}|\beta_e,\alpha_n\rangle + c^{\beta}|\beta_e,\beta_n\rangle \\
|\lambda_3\rangle &= |\alpha_e,\alpha_n^*\rangle = c^{\alpha}|\alpha_e,\alpha_n\rangle + s^{\alpha}|\alpha_e,\beta_n\rangle \\
|\lambda_4\rangle &= |\alpha_e,\beta_n^*\rangle = -s^{\alpha}|\alpha_e,\alpha_n\rangle + c^{\alpha}|\alpha_e,\beta_n\rangle.
\end{aligned} \tag{26}$$

For $A^{\pm}/4 \ll \omega_n$ the values of the coefficients become

$$c^{\beta/\alpha} \cong 1 - \frac{1}{2}\left(\frac{|A^+|}{4\omega_n}\right)^2 \cong 1; \quad s^{\beta/\alpha} \simeq \frac{|A^+|}{4\omega_n}, \tag{27}$$

and the energies of Λ_0, using perturbation theory up to second order are given by:

$$\begin{aligned}
\lambda_1 &= \frac{1}{2}\left(-\Delta\omega_e - \omega_n - \frac{1}{2}A_z - \frac{1}{8}|A^+|^2 \Big/ \omega_n\right) \\
\lambda_2 &= \frac{1}{2}\left(-\Delta\omega_e + \omega_n + \frac{1}{2}A_z + \frac{1}{8}|A^+|^2 \Big/ \omega_n\right) \\
\lambda_3 &= \frac{1}{2}\left(\Delta\omega_e - \omega_n + \frac{1}{2}A_z - \frac{1}{8}|A^+|^2 \Big/ \omega_n\right) \\
\lambda_4 &= \frac{1}{2}\left(\Delta\omega_e + \omega_n - \frac{1}{2}A_z + \frac{1}{8}|A^+|^2 \Big/ \omega_n\right).
\end{aligned} \tag{28}$$

As follows from Eq. (26) the $|\lambda_k\rangle$ states are almost pure product states. As a consequence the EPR spectrum is composed of two lines, at $\Delta\omega_e = \pm\frac{1}{2}A_z$, the DQ spectrum of one line, at $\Delta\omega_e = \omega_n + \frac{1}{8}|A^+|^2/\omega_n$, and the ZQ spectrum of one line, at $\Delta\omega_e = -\omega_n - \frac{1}{8}|A^+|^2/\omega_n$. The NMR spectrum contains two lines at $\omega_n \mp \frac{1}{2}A_z + \frac{1}{8}|A^+|^2/\omega_n$.

The same diagonalization applied to the MW term H_{MW} results in Λ_{MW}, with effective MW fields of magnitudes

$$\omega_{1,3} = \omega_{2,4} = (c^{\beta}c^{\alpha} - s^{\beta}s^{\alpha})\omega_1 \simeq \omega_1 \tag{29}$$

for the allowed EPR transitions, and

$$\omega_{1,4} = \omega_{2,3} = (s^{\alpha}c^{\beta} + c^{\beta}s^{\alpha})\omega_1 \equiv s\omega_1 \simeq \frac{|A^+|}{2\omega_n}\omega_1 \tag{30}$$

for the DQ ($2 \to 3$) and the ZQ ($1 \to 4$) transitions. The scale factor s is inversely proportional to the external field, and is invariant to the type of nucleus (for a fixed *e*–*n* distance). Thus, irradiation at the DQ or ZQ transition, corresponding in the rotating frame to an off-resonance irradiation at $\Delta\omega_e \cong \pm\omega_n$, results in an effective MW irradiation of $\omega_{1,DQ/ZQ} \simeq s\omega_1$ that is on-resonance for the DQ/ZQ transitions, with $\Delta\omega_{DQ/ZQ} = \Delta\omega_e \mp \omega_n \simeq 0$. At this condition the MW irradiation is far off-resonance from the SQ EPR transitions, and its effect on the transition can be ignored as long as $\omega_1^2 T_{1,e} \ll \omega_n^2 T_{2,e}^{-1}$.

The normalized equilibrium populations of our two-spin system can be expressed as

$$\begin{aligned}
p_1^{\Lambda}(0) &= p_2^{\Lambda}(0) = \frac{1}{2}\frac{1}{1+\varepsilon_e}, \\
p_3^{\Lambda}(0) &= p_4^{\Lambda}(0) = \frac{1}{2}\frac{\varepsilon_e}{1+\varepsilon_e},
\end{aligned} \tag{31}$$

with ε_e the electron Boltzman factor $\exp(-\hbar\omega_e/k_BT)$. To simplify the derivations we ignore here the nuclear Boltzman factor. As a result the nuclear polarization, equal to $P_n = \frac{1}{2}(p_1^{\Lambda} - p_2^{\Lambda} + p_3^{\Lambda} - p_4^{\Lambda})$, and the electron polarization, equal to $P_e = \frac{1}{2}(p_1^{\Lambda} - p_3^{\Lambda} + p_2^{\Lambda} - p_4^{\Lambda})$, are at thermal equilibrium

$$\begin{aligned}
P_n(0) &\simeq 0, \\
P_e(0) &= \frac{1}{2}\frac{1-\varepsilon_e}{1+\varepsilon_e}.
\end{aligned} \tag{32}$$

To evaluate the nuclear polarization during irradiation of the DQ transition we must take into account the values of the DQ ($2 \to 3$) MW irradiation together with its $T_{2,DQ}^{-1}$ and $T_{1,DQ}^{-1} = T_{1,23}^{-1}$ relaxation rates as well as of $T_{1,e}^{-1}$, $T_{1,ZQ}^{-1} = T_{1,14}^{-1}$ and $T_{1,n}^{-1} = T_{1,12}^{-1} = T_{1,34}^{-1}$. According to the steady state Bloch equations, this MW irradiation will result in a steady state end population difference:

$$\{p_2(t) - p_3(t)\} = \frac{1 + (\Delta\omega_{DQ}T_{2,DQ})^2}{1 + (\Delta\omega_{DQ}T_{2,DQ})^2 + (s\omega_1)^2 T_{1,DQ}T_{2,DQ}}\{p_2(0) - p_3(0)\}, \tag{33}$$

for all $t \gg T_{1,DQ}$. Thus, the DQ irradiation creates a non-Boltzman distribution of populations, which results in $p_2(t) = p_3(t)$ when the saturation condition $s^2\omega_1^2 \gg T_{1,DQ}^{-1}$. $T_{2,DQ}^{-1}$ is fulfilled at $\Delta\omega_{DQ} = 0$. (A similar expression can be derived for the irradiation on the ZQ ($1 \to 4$) transition).

For an electron $T_{1,e}$ that is much higher than the other relaxation rates, the SQ transitions will reach the steady state ratios for $t \gg T_{1,e}$:

$$\frac{p_3(t)}{p_1(t)} = \frac{p_4(t)}{p_2(t)} = \varepsilon_e. \tag{34}$$

Combining these ratios with the DQ saturation $p_2(t) = p_3(t)$, will give by a straightforward calculation the steady state polarizations:

$$\begin{aligned}
P_n(t) &= \frac{1}{2}\frac{1-\varepsilon_e}{1+\varepsilon_e} = P_e(0), \\
P_e(t) &= \frac{1}{2}\frac{1-\varepsilon_e}{1+\varepsilon_e} = P_e(0).
\end{aligned} \tag{35}$$

In a similar manner saturation of the ZQ transition results in $p_1\ (t) = p_4(t)$ and together with Eq. (34) we reach the end polarizations:

$$P_n(t) = -P_e(t) = -P_e(0). \tag{36}$$

Thus in these ideal cases the nuclear and electron polarizations become equal in magnitude and the nuclear enhancements becomes $\pi_e = \pm 1$ for irradiation of the DQ or ZQ transitions, respectively. At high temperatures (above ~10 K at 3.3 T) this results in about $\pi_n = \pm\gamma_e/\gamma_n$ (A similar derivation can be found in [44]). In summary, the SE mechanism results in a re-distribution of the populations, such that in the ideal case the nucleus becomes polarized while the electron maintains its initial polarization.

In the presence of high nuclear relaxation rates, the nuclear relaxation process together with the saturation of the DQ or ZQ transition will drive the nuclear polarizations back to their nuclear Boltzman distribution at $t \gg T_{1,n}, T_{1,ZQ}$

$$\frac{p_2(t)}{p_1(t)} = \frac{p_4(t)}{p_3(t)} = \varepsilon_n \simeq 1, \tag{37}$$

and when the DQ/ZQ cross relaxation rates increase the system returns to its electron Boltzman distribution

$$\frac{p_3(t)}{p_2(t)} = \varepsilon_e \quad \text{or} \quad \frac{p_4(t)}{p_1(t)} = \varepsilon_e, \tag{38}$$

for DQ or ZQ irradiation, respectively. Both relaxation processes are counter active to the action of $T_{1,e}^{-1}$ and the relative values of $T_{1,n}^{-1}$ and $T_{1,DQ/ZQ}^{-1}$ with respect to $T_{1,e}^{-1}$ determine the final polarizations. This will result in a depletion of the end polarizations, $|P_n(t)|$, $P_e(t) < P_e(0)$, when the condition $T_{1,e}^{-1} \gg T_{1,n}^{-1}$, $T_{1,DQ/ZQ}^{-1}$ is not met. This was experimentally demonstrated in a recent publication [45].

Additionally, high $T_{1,n}^{-1}$ and $T_{1,DQ/ZQ}^{-1}$ rates will prevent the irradiated states from reaching saturation, resulting in $P_n(t) < P_e(t)$. The effect of $T_{1,n}^{-1}$ can be understood as an effective $T_{1,DQ/ZQ}^{-1}$ relaxation in Eq. (33), generated from it's combination with $T_{1,e}$. For example, when $T_{1,n}^{-1} \ll T_{1,DQ}^{-1}$ the DQ spin–lattice relaxation rate $T_{1,DQ}^{-1}$ in Eq. (33) should be replaced by $T_{1,n}^{-1}$.

The effect of $T_{2,DQ/ZQ}^{-1}$ on the nuclear polarization is evident from Eq. (33), where lowering of these rates results in an increased polarization when $\Delta\omega_{DQ/SQ} \simeq 0$. Similarly, a decrease in the value of $T_{2,e}^{-1}$, or more correctly in that of $T_{1,e}^{-1}T_{2,e}^{-1}$, will increase the influence of the MW field on the main EPR lines. This will result in a lowering of the electronic polarization, which in turn reduces the end nuclear polarization.

4.1.2. Simulations of polarization enhancements

We will now show some results of the time dependence of the polarizations of the *e–n* system during MW irradiation, obtained by Liouville space calculations. These calculations were performed using a self-written MATLAB (MathWorks ©) based program. The interaction and relaxation parameters used for these calculations are given in Table 1 and in the figure captions. In all calculations the nucleus has the γ_n value of a proton. Unless stated otherwise, we chose that $T_{1,DQ/SQ}^{-1} \ll T_{1,n}^{-1}$ and in all cases $A_z \ll \omega_n$. At the start we show in Fig. 4 the nuclear polarization as a function of $\Delta\omega_e$, after a long MW irradiation of an intensity $\omega_1/2\pi = 0.1$ kHz. This is shown for (a) for a single *e–n* pair, and in (b) for a sum of *e–n* spin systems, where the *g*-tensor of the electrons was randomly oriented. The principal values of the *g*-tensors of all systems are $g_{xx} = 2.0034$, $g_{yy} = 2.0031$, and $g_{zz} = 2.0027$ MHz, similar to the values of trityl radicals [37]. The blue insert in the figure shows the corresponding EPR spectrum.

In Fig. 5a the build up with time of the polarizations are shown for two MW irradiation fields applied at the DQ transition. For these simulations the MW nutation frequencies were set equal to $\omega_1/2\pi = 0.1$ MHz (solid lines) and 0.02 MHz (dashed lines), where only the first satisfies the saturation condition. While for $\omega_1/2\pi = 0.1$ MHz the build up time during the MW irradiation on the DQ transition is much faster than $T_{1,n}^{-1}$, for $\omega_1/2\pi = 0.2$ MHz they are of a similar time-scale. This last case is accompanied by a decrease of the end nuclear polarization. In Fig. 5b the time dependence of the populations of the four-level system are shown, demonstrating the ability of the MW to saturate the $|a_e, \alpha_n^*\rangle \rightarrow |\beta_e, \beta_n^*\rangle$ transition, while $T_{1,e}^{-1}$ effects the populations by bringing them to the ratios given in Eq. (34). Changes in the values of T_{2n}^{-1} ($\leqslant T_{2e}^{-1}$) and A_z ($\ll\omega_n$) had no observable effects on the results shown here.

Modifying the $T_{1,n}^{-1}$ and the $T_{1,DQ}^{-1} = T_{1,ZQ}^{-1}$ rates, for an on-resonance DQ irradiation with $\omega_1/2\pi = 0.1$ MHz, results in end nuclear polarizations that are shown in Fig. 6. Here we restricted ourselves

Table 1
The interaction and relaxation parameters used during the simulations. All other parameters, and modifications of the values given here, are given in the figure captions.

Parameter	Value
$A_{z,1}/2\pi$	−0.46 MHz
$A_1^+/2\pi$	1.38 MHz
ω_n[a]$/2\pi(^1H)$	144 MHz
$\Delta\omega_e$	ω_n
ω_1	0.1 MHz
$T_{1,e}$	10 ms
$T_{1,n}$	2 s
$T_{1,DQ/ZQ}$[b]	10^3 s
$T_{2,e,DQ,ZQ}$	10 μs
$T_{2,n}$	1 ms

[a] Unless stated otherwise in the figure captions, simulations were performed using ^{1}H spins. $\omega_n/2\pi = 36$ MHz was used for ^{13}C spins.
[b] This value was used for the *e–n* system, unless stated otherwise in the figure captions. For the multi-nuclei systems $T_{1,DQ/ZQ}$ was calculated from $T_{1,e}$, as explained in the text.

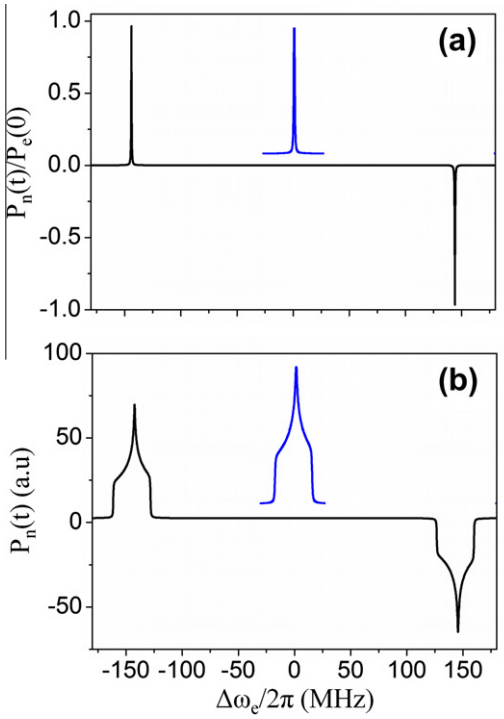

Fig. 4. The nuclear polarization (black) as a function of $\Delta\omega_e$, due to a long MW irradiation. The polarizations were calculated for (a) a single *e–n* spin pair, and (b) a sum of *e–n* spin pairs, with the parameters taken from Table 1. In (b) the orientation of the *g*-tensor of the electron, with principal components $g_{xx} = 2.0034$, $g_{yy} = 2.0031$, and $g_{zz} = 2.0027$ MHz, was varied and the polarizations, obtained for 52,274 pairs of α and β ROSELEB angles over a full sphere [46] [47], were added together. The blue inserts in the figure show the corresponding EPR spectrum.

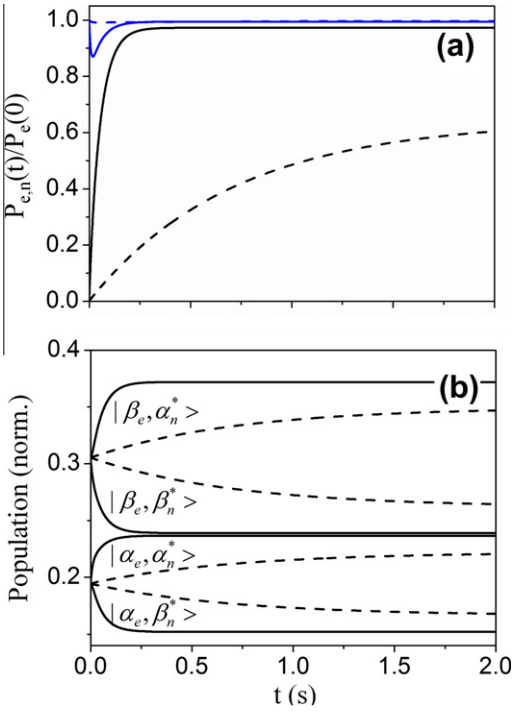

Fig. 5. The time evolution of the polarizations and populations, during a long *DQ* MW irradiation on an *e*–*n* spin system. The calculations were performed for a MW irradiation strengths of 0.1 MHz (solid lines) and 0.02 MHz (dashed lines). The interaction and relaxation parameters were taken from Table 1. The polarizations of the nucleus (black) and electron (blue) are plotted in (a) and the corresponding populations of the eigenstates in (b).

to $T_{1,DQ}^{-1}$, $T_{1,n}^{-1} \leqslant T_{1,e}^{-1}/10$. At high values of these rates the MW irradiation can not saturate the DQ transition, and the end nuclear polarization is reduced. The fact that this contour looks symmetric demonstrates the similarity of the effects of $T_{1,n}^{-1}$ and $T_{1,ZQ}^{-1}$ on the nuclear polarization as long as $T_{1,DQ}^{-1}$, $T_{1,n}^{-1} < T_{1,e}^{-1}$. In what follows we will therefore only consider the influence of $T_{1,n}^{-1}$ on $P_n(t)$, with $T_{1,DQ}^{-1} \ll T_{1,n}^{-1} < T_{1,e}^{-1}$.

To demonstrate the dependence of the nuclear and electron polarizations on the MW field intensity at the DQ transition, we

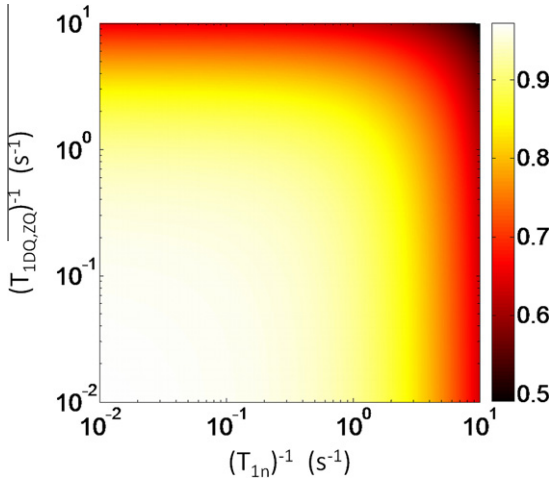

Fig. 6. The effect of the nuclear and DQ/ZQ spin–lattice relaxation rates on the DNP end polarization of the nucleus in an *e*–*n* spin system. The colorbar represents the value of $P_n(t)/P_e(0)$. The interaction and all other relaxation parameters used for the simulations were taken from Table 1. The relaxation rates were kept in the range $T_{1,e}^{-1}/10 \geqslant T_{1n,DQ,ZQ}^{-1}$, with $T_{1,DQ}^{-1} = T_{1,ZQ}^{-1}$ in all cases.

show end polarizations as a function of $\omega_1/2\pi$ in Fig. 7a. for two $T_{1,n}^{-1}$ values, 2 s and 10 s. Up to saturation the end nuclear polarization is as expected from the solution of the steady state solution of the Bloch equations in Eq. (33). A decrease in $T_{1,n}^{-1}$ results in a shift of the saturation condition, $s^2\omega_1^2 \gg T_{1,n}^{-1}T_{2,DQ}^{-1}$, and thus a shift of the ω_1-dependence of the polarization. At high MW powers the nuclear and electronic polarizations decrease due to off-resonance irradiation of the main EPR lines. In Fig. 7b the dependence of the polarization buildup time t_R as a function of ω_1 is drawn. Here t_R is the time it takes for the nuclear polarization, P_n, to reach $(1-e^{-1})$ of its final value, $P_n(t_R) = (1-e^{-1})[P_n(t) - P_n(0)] + P_n(0)$, with $t \gg T_{1,n,DQ}$. For low MW intensities the buildup time becomes similar to $T_{1,n}^{-1}$. At higher MW intensities, neglecting the effect of the off-resonance irradiation on the main EPR transitions, t_R becomes shorter, almost following the value of $(s\omega_1)^{-2}T_{2,DQ}^{-1}$ (Eq. (23)), until it reaches the limiting $T_{1,e}$ value.

Finally the off-resonance effect around the DQ transition is examined for different MW intensities. Once again, the off-resonance dependent nuclear end polarization profile in Fig. 8 shows a Lorentzian lineshape. Its linewidth can become of much importance when DNP enhancement experiments are performed on samples with a large anisotropic *g*-tensor. The polarization buildup time is again close to $T_{1,n}$ for large $\Delta\omega_{DQ}$ values, in analogy to the on-resonance irradiation at low MW intensities.

4.2. Multiple core nuclei

Up to this point we considered only a single core nucleus. We will now extend our discussion to multiple core nuclei surrounding

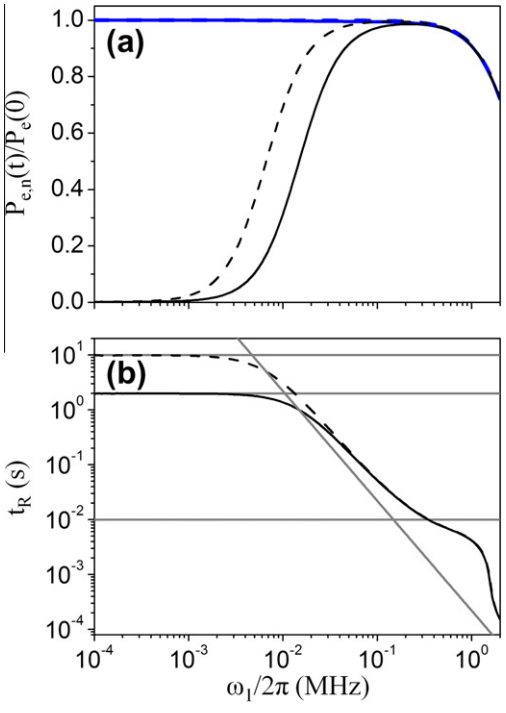

Fig. 7. The effect of the MW irradiation field strength on the steady state end polarizations and buildup times, for an on-resonance irradiation of the *DQ* transition of an *e*–*n* spin system. The value of $T_{1,n}^{-1}$ was chosen equal to 0.5 s^{-1} (solid lines) and 0.1 s^{-1} (dashed lines), with all other parameters taken from Table 1. In (a) the nuclear (black lines) and electron (blue lines) end polarizations are plotted. In (b) the nuclear buildup time t_R is plotted. The three gray horizontal lines (top to bottom) indicate the values of the two nuclear relaxation rates $T_{1,n}^{-1}$ and the electron relaxation rate $T_{1,e}^{-1}$. The decaying straight line follows the expression $(s\omega_1)^{-2}T_{2,DQ}^{-1}$.

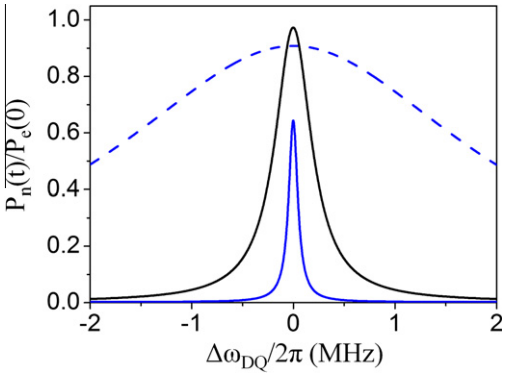

Fig. 8. Nuclear polarization as a function of the off-resonance value $\Delta\omega_{QD}$, around the *DQ* transition at $\Delta\omega_{DQ} = \Delta\omega_e - \omega_n$. The polarization profiles were calculated for an *e*–*n* spin system, using $\omega_1/2\pi$ values of 0.02 MHz (solid blue line), 0.1 MHz (solid black line), and 1 MHz (dashed blue line). All other parameters were taken from Table 1.

a single electron. In what follows we present the main features of the SE-DNP process that are influenced by the *hfi* terms coupling the electron with all nuclei in the system. As in the two-spin case, the DNP polarization enhancement is a result of the interplay between the MW irradiation field and the spin–lattice relaxation parameters. The spin state dimension of the multi-core system complicates the evaluations of the individual nuclear polarizations and we will show only results from systems with up to nine-spins. Some issues concerning the polarization transfer from the core nuclei to the bulk nuclei will also be mentioned at the end of the discussion, but will not be the focus of this publication.

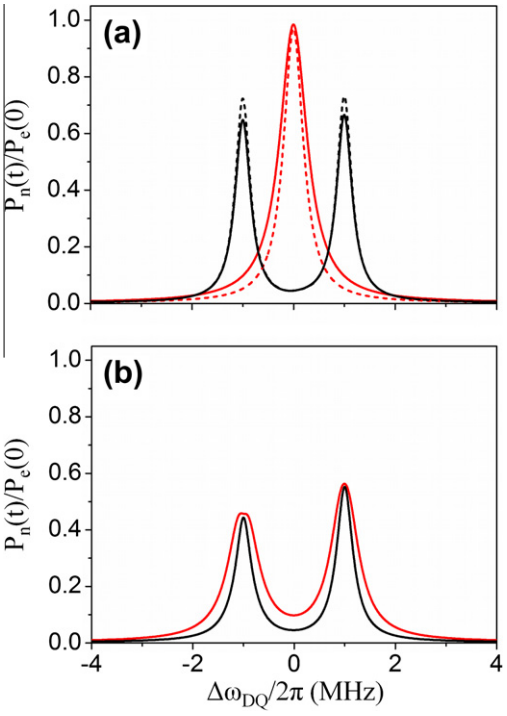

Fig. 9. The nuclear polarizations during a SE-DNP experiment on an e–n_2 system, as a function of the MW frequency around the DQ transitions. The polarizations of the nuclei are given by the black (nucleus-1) and red (nucleus-2) lines, respectively. The secular *hfi* coefficients during the simulations were $A_{z1} = 0$, and $A_{z2} = 2$ MHz in (a) and $A_{z1} = A_{z2} = 2$ MHz in (b), respectively with the pseudo-secular coefficients $A_1^{\pm} = 1.38$ MHz, and $A_2^{\pm} = 2.11$ MHz in (a) and (b). The nuclear relaxation rate of nucleus-1 was $T_{1,1}^{-1} = 0.5\ s^{-1}$. For nucleus-2 $T_{1,2}^{-1} = 0.5\ s^{-1}$ (solid lines) and $T_{1,2} = 1\ s^{-1}$ (dashed lines) were used. The nuclear dipolar interaction was neglected in all cases. All other parameters were taken from Table 1.

4.2.1. The DQ and ZQ spectra

We start by considering a system with a single electron hyperfine coupled to N_c core nuclei. At first we will discuss the possible polarization enhancements of all nuclei in the system. To simplify this discussion we ignore for the time being all mutual nuclear dipole–dipole interactions. Thus the Hamiltonian of our system contains only the Zeeman interactions H_Z and the hyperfine interactions H_{hfi}. Because the last is small with respect to the nuclear Zeeman interaction, diagonalization of the form

$$\Lambda_0 = D^{-1}(H_Z + H_{hfi})D \tag{39}$$

will mix the original product states $|\alpha_e,M\rangle$ and $|\beta_e,M\rangle$, with $M = -\frac{1}{2}N_c,\ldots,\frac{1}{2}N_c$, only in a minor fashion. This state mixing was represented before by adding an asterix to M^*, and the eigenfunctions almost maintain their original product state form. There are 2^{N_c-1} DQ (or ZQ) transitions for each nucleus i that correspond to a simultaneous interchange between $\beta_e - \alpha_e$ and $\beta_i - \alpha_i$ (or $\alpha_i - \beta_i$), with a total of $N_c \times 2^{N_c-1}$ DQ (or ZQ) transitions. The 2^{N_c-1} lines composing the DQ (or ZQ) spectra of a single spin have frequencies $\Delta\omega_{DQ,i}$ (or $\Delta\omega_{ZQ,i}$) that can easily be evaluated, taking only the secular part of H_{hfi} into account:

$$\Delta\omega_{DQ,i} = \Delta\omega_e - \omega_n + \frac{1}{2}\sum_{\{a_j\}=\pm1,j\neq i} a_j A_{z,j} \tag{40}$$

$$\Delta\omega_{ZQ,i} = \Delta\omega_e + \omega_n + \frac{1}{2}\sum_{\{a_j\}=\pm1,j\neq i} a_j A_{z,j}$$

where $\{a_j\} = \pm1$ presents all 2^{N_c-1} permutations of all nuclei $j \neq i$. The spread of the transitions of the DQ (or ZQ) spectra corresponding to nucleus i are therefore determined by the sum of all $|A_{z,j}|$ values of all other nuclei, $j \neq i$. Thus the overall width of the spectrum of each i will mainly depend on the *hfi* of the core nuclei j closest to the electron. Furthermore, the spread of frequencies for nuclei close to the electron will be smaller than those of far nuclei. These

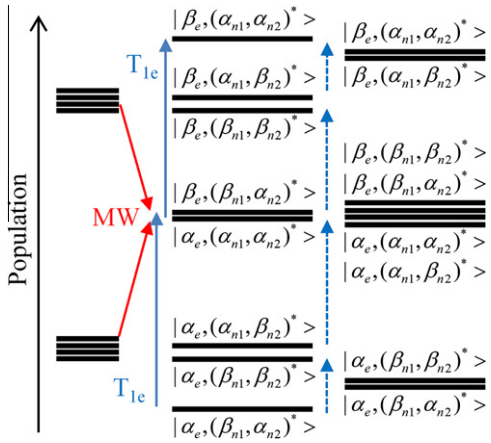

Fig. 10. A schematic representation of the populations of a e–n_2 spin system during a SE-DNP experiment, where only one of the DQ transitions is irradiated. The MW irradiation is assumed to affect only the transition $|\alpha_e,(\alpha_{n1},\alpha_{n2})^*\rangle \rightarrow |\beta_e,(\beta_{n1},\alpha_{n2})^*\rangle$, corresponding to one of the two DQ transitions of nucleus-1. The astrix * indicates the small *hfi* state mixing. The left column shows the thermal equilibrium populations (not in the right scale) of the e–n_2 system. The red arrows indicate the equilibration of the populations corresponding to the DQ irradiation. The middle column represents the populations after the saturation of the irradiated transition and the action of $T_{1,e}^{-1}$ (blue arrows). The later influences the positions of the irradiated levels and the highest and lowest populations in the middle column. The other four populations maintain their initial values. Introducing nuclear relaxation result in an additional shift of the population. Here we assumed that the nuclei have different relaxation rates: $T_{1,e}^{-1} \gg T_{1,2}^{-1} \gg T_{1,1}^{-1}$. The effect of $T_{1,2}^{-1}$ (dashed blue arrows), in combination with the MW irradiation and $T_{1,e}^{-1}$ relaxation, is shown in the right column. In this special case, irradiation of a single DQ transition of spin-1 can still result in a polarization with $\pi_{e;1} = 1$.

frequency spreads are on the order of the total DQ (or ZQ) EPR line width, which in general is much larger than the effective DQ (or ZQ) MW irradiation field.

In Eq. (40) we ignored the small shift in the energies resulting from the pseudo-secular terms $A_i^{\pm}S_zI_i^{\pm}$. However, these terms are the origin of the MW irradiation of the DQ (or ZQ) transitions. Since the $A_{c_i}^{\pm}S_zI_{c_i}^{\pm}$ terms commute with each other, the pairs of states that differ only in α_i and β_i will mix according to Eq. (26) and result in an effective irradiation strength $s_i\omega_1$ of the form given in Eq. (27).

4.2.2. The nuclear polarizations

To demonstrate the potential of the SE-DNP nuclear enhancement process let us consider an ideal situation, in which the MW irradiation field could excite and saturate all DQ transitions in the system and $T_{1,e}^{-1} \gg T_{1,n,DQ,ZQ}^{-1}$ for all transitions. Neglecting the dipolar interactions between the nuclei, it can be shown that in this ideal case the polarization of each nucleus i becomes $P_i(t) = \pm P_e(0)$ for DQ and ZQ irradiation, respectively (see Appendix A). Introduction of the dipolar interactions complicates this derivation. It's effect will be discussed later using simulations.

In practice the MW field is not strong enough to saturate all DQ or ZQ transitions. Even if we assume that the effective irradiation $s\omega_1$ for the transitions is sufficient to saturate the DQ transitions on-resonance $s\omega_1 T_{1,DQ}T_{2,DQ} \gg 1$, the transitions at an off -resonance values of

$$\Delta\omega_{DQ} = s_i\omega_1\sqrt{T_{1,DQ}/T_{2,DQ}}, \tag{41}$$

will be saturated only by 50% and for larger values by much less. When we consider the ^{1}H sample used in Fig. 2a, and choose the values $s_i\omega_1/2\pi = 1$ kHz, $T_{2,DQ} = 5$ μs and $T_{1,DQ} = 1$ s, we can see that only a small part of these transitions will be excited, and we can not expect large nuclear polarizations. We can expect an improvement for smaller γ-values and nuclear concentrations. This can be seen clearly in Fig. 2b, where a ^{13}C sample is considered. Reduction of the nuclear concentration of the whole sample has however some drawbacks. It diminishes the number of (observable) hyperpolarized nuclei, it possibly lowers the scale factors s_i, and decreases the dipolar interactions, responsible for the bulk polarization *via* spin diffusion. It may therefore be desired to remove only nuclei close to the electron, for example by deuteration during ^{1}H-DNP experiments or low ^{13}C enrichment isotope labelling, during ^{13}C-DNP experiments. In the next section examples of reduced end polarizations will be demonstrated for a small core configuration.

4.2.3. The polarizations of an e–n_2 system

After discussing the general features of a system of core nuclei located around a single electron, we will now show some numerical results that demonstrate the interaction and relaxation parameter dependence of the nuclear polarizations. As a start let us consider a simple three-spin model system with one electron coupled to two nuclei ($i = 1, 2$), that are not dipolar coupled. The values of the *hfi* coefficients we have chosen for this system are $A_{z,1} = 0$, $A_1^{\pm} = 1.38$ MHz, and $A_{z,2} = 2$ MHz, $A_2^{\pm} = 2.11$ MHz. As a result the DQ spectrum of nucleus-2 consists of one line and that of nucleus-1 of two lines. All other parameters are given in Table 1, with $T_{1,1}^{-1} = T_{1,2}^{-1} = 0.5\ s^{-1}$. while the $T_{1,kk'}^{-1}$ rates were derived following the discussion in Section 2.1, assuming the linear operators, S_x and $I_{x,i}$, are the source of the relaxation mechanism. We note here that during all our simulations the initial thermal equilibrium nuclear polarizations are determined by Eq. (21), including $\varepsilon_n < 1$. The parameters of the e–n_2 system are chosen such that for an e–n system with the parameters of nucleus-1 or nucleus-2 the end polarization will be $P_e(0)$.

Following the above discussions, we expect that the polarization of nucleus-1, when irradiated at one of its DQ transitions $\Delta\omega_e = \omega_n \pm \frac{1}{2}A_{z,2}$, will reach only $P_e(0)/2$. In Fig. 9a (solid lines) the end polarizations of the two-spins, after a DQ irradiation, are shown as a function of the off-resonance value $\Delta\omega_{DQ} = \Delta\omega_e - \omega_n$. The $P_2(t)$ value reaches a value close to $P_e(0)$, but $P_1(t)$ exceeds $P_e(0)/2$. An increase of $T_{1n,2}^{-1}$ by a factor of 2 changes the off-resonance dependence of the end $P_1(t)$ as is shown Fig. 9a (dashed line).

The reason for the unexpected value of the $P_1(t)$ polarization is a result of the presence of the nuclear $T_{1,n}^{-1}$'s. The combined action of the MW irradiation on one of the DQ satellites of spin-1 together with the $T_{1,2}^{-1}$ of spin-2 has a constructive effect on $P_1(t)$. This can be understood best when we consider the extreme situation $T_{1,1}^{-1} \ll T_{1,2}^{-1} \ll T_{1,e}^{-1}$ which results in an end $P_1(t)$ that approaches $P_e(0)$ during DQ irradiation of one of the spin-1 satellites only. This is schematically demonstrated in Fig. 10, where the evolution of the populations of our eight-level system is followed under the influence of the MW field (together with $T_{2,e}^{-1}$), $T_{1,e}^{-1}$ and $T_{1,2}^{-1}$.

An irradiation at the frequency of a DQ transition corresponding to one particular nucleus polarizes only that nucleus, as is evident from Fig. 9a. However when the DQ transitions of both nuclei have similar frequencies, the polarizations of the two nuclei become dependent on each other. This effect is demonstrated in Fig. 9b, where we choose an exact overlap of DQ satellites with $A_{z,1} = A_{z,2} = 2$ MHz. At this condition the maximum end polarizations decrease with respect to those in Fig. 9a. This simple calculation demonstrates the importance of performing the calculations on the populations of the different quantum states, rather then on the polarizations of the different nuclei.

4.2.4. The polarizations of an e–n_8 system

We now extend our simulations and consider a spin system with one electron and $N_c = 8$ nuclei. These calculations were performed using the Hilbert space approach discussed in Section 3.2. We chose a two-dimensional (x,z) spin system, as shown in the inserts of Fig. 11, with the *hfi* terms and dipolar parameters calculated by relative positions of the spins. The external magnetic field points in the z-direction. In Fig. 11a and c we show the steady state end polarizations of all nuclei as a function of the DQ MW off-resonance value $\Delta\omega_{DQ} = \Delta\omega_e - \omega_n$. These simulations were performed without (a) and with (c) the nuclear dipole–dipole interactions taken into account. A constant nuclear spin–lattice relaxation time of $T_{1,i}^{-1} = 0.5\ s^{-1}$ was used for all nuclei with $i = 1,\ldots,N_b$ and the $T_{1,kk'}^{-1}$ rates were evaluated assuming that the linear operators S_x and $I_{x,i}$ are the source of relaxation.

To understand the results of these simulations we must realize that the two nearest nuclei (red and magenta) have about equal secular hyperfine terms. This results in two bands in their DQ spectrum, while the DQ spectra of the other nuclei consist of three bands. Each band is composed of many DQ transitions, with frequencies determined by the *hfi* of all other nuclei. Looking at the remote nuclei, the DQ central band has a higher transition density than the two other bands, which results in Fig. 11a in higher polarizations. The band structure of the polarization profiles are a consequence of the (small) size of our system. In reality, when many spins are involved and we are dealing with amorphous samples, there will not be any band structure. This can be seen in the DQ and ZQ EPR spectrum in Fig. 2. In general, the effective MW irradiation field decreases for increasing distance, and when coordinates of the nucleus approach $x_i = 0$ or, $z_i = 0$. These arguments explain the features of the individual polarizations in Fig. 11a and c.

The introduction of the dipolar interaction results in an increase in the polarizations of those nuclei i that are coupled to neighbors j

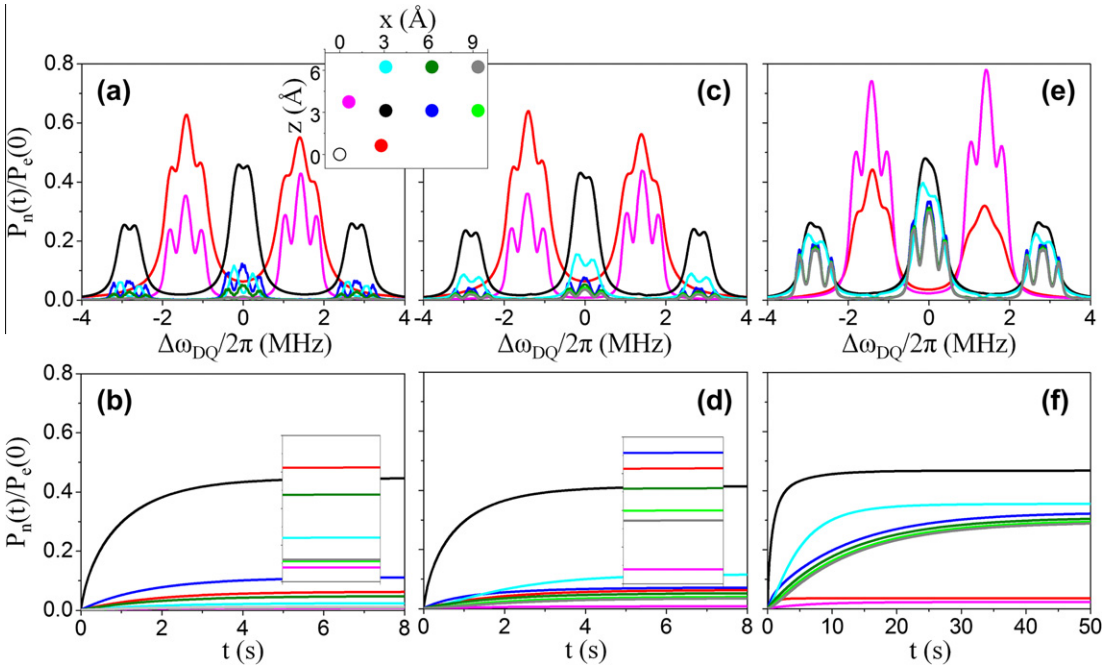

Fig. 11. The nuclear polarizations during a DQ SE-DNP experiment on an e–n_8 system. The nuclei are arranged in the x–z plane, as shown in the insert, with the external magnetic field pointing in the z-direction. The nuclei are marked by different colors, and their coordinates are determined relative to the electron (open circle) at the origin. The colors on the polarization profiles correspond to the color of the nuclei in the insert. The simulations were performed without (a and b) and with (c–f) taking the nuclear dipole–dipole interactions into account. In (a–d) nuclear relaxation rates of $T_{1,n}^{-1} = 0.5\ s^{-1}$ were used for all nuclei. In (e and f) the $T_{1,i}$ values were calculated for each nuclei i using $T_{1,i} = (A_i^{\pm})^2 T_{1A}^{-1} + T_{1,n,0}^{-1}$, with $T_{1A}^{-1} = 0.2\ s^{-1}$ and $T_{1,n,0}^{1} = 0.05\ s^{-1}$. In (a, c, e) the steady state end polarizations are drawn as a function of the MW frequency around the DQ transitions. In (b, d, f) the buildup of the polarizations with time are shown, for MW irradiation at $\Delta\omega_{DQ} = \Delta\omega_e - \omega_n = 0$. The inserts in (b and d) correspond to a $\times 10$ magnification of the end polarization. Note the change in time-scale in (f). The *hfi* coefficients of the nuclei, going from left to right and from bottom to top, are $A_z = [2.86, -2.78, -0.46, 0.09, -0.33, -0.06, 0.060.004]$ MHz and $A^{\pm} = [2.11, 0.70, 1.38, 0.28, 0.28, 0.17, 0.07, 0.08]$ MHz. The dipolar interactions between nearest neighboring nuclei are all in the order of 4 or 2 kHz. The nuclei marked in black have the same hyperfine coefficients as in Figs. 4–8, and the same effective irradiation as nuclei 1 in Fig. 9 (black line). All other parameters are as given in Table 1. The calculation was performed using the Hilbert space model.

with similar A_{zj} values. This can be observed from a comparison between Fig. 11a and c, where the dipole–dipole interaction between the nuclei is added to the simulations only in the later. Fig. 11b and d shows the polarization buildup with time, for a DQ MW irradiation at $\Delta\omega_{DQ} = 0$, using the same parameters as in Fig. 11a, c, respectively. In both cases the polarization reaches its steady state in a time of the order of $T_{1,n}$.

Let us now introduce a relaxation mechanism that relies on the hyperfine terms of the laboratory Hamiltonian, in a e–n_8 spin system with parameters as in Fig. 11c and d. Because of the distance dependence of the *hfi* coefficients, this relaxation mechanism will create a gradient in the effective $T_{1,i}^{-1}$ values with $i = 1,\ldots,N_b$. For thermal fluctuations, or by considering $T_{1,e}^{-1}$ as the correlation time of motion, of the interaction terms that are determined by $A_i^{\pm} S_z I_i^{\pm}$, we can evaluate single transition $T_{1,kk'}^{-1}$'s by starting with single nuclear spin–lattice relaxation rates $T_{1,i}^{-1} = (A_i^{\pm})^2 T_{1A}^{-1} + T_{1n0}^{-1}$ and following the derivation introduced in Section 2.1. In our simulations we have taken $T_{1A}^{-1} = 0.2\ s^{-1}$ and a constant $T_{1,n0}^{-1} = 0.05\ s^{-1}$. The result for the polarizations in this case are shown in Fig. 11e and f. Interestingly, the spins with the higher relaxation rates (e.g. with shorter electron–nuclear distances) have lower end polarizations than their values in Fig. 11c and d, while more removed nuclei have enlarged end polarizations. These relaxation parameters result in a decrease in the buildup times of the polarization when compared with these times in Fig. 11b and d (Note the change in the time axis in Fig. 11f relative to Fig. 11b and d). Similar results were obtained from calculations of the polarization profiles with $A_{z,i} S^{\pm} I_i^{\pm}$ and $A_i^{2\pm} S^{\pm} I_i^{\mp}$ as our relaxation source (data not shown). This again shows the similarity of the effects of $T_{1,n}^{-1}$ and $T_{1,DQ}^{-1}$ on the end polarizations, as discussed around Fig. 6. These results give us a glimpse of the complex dependence of the SE-DNP enhancement process on the relaxation parameters.

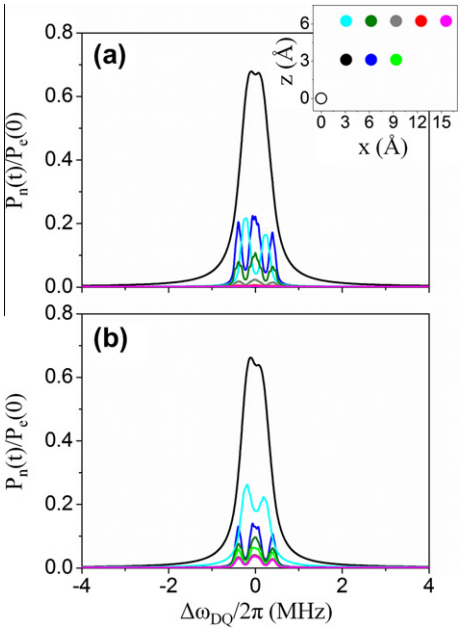

Fig. 12. The steady state end nuclear polarizations during a DQ SE-DNP experiment on an e–n_8 spin system. The nuclear system differs from the one in Fig. 11. Here the two nuclei closest to the electron are moved to positions removed from the electron, as can be seen in the insert. The effect of the removal of the two nearest nuclei on the populations can be observed clearly by comparing the end state polarizations with their values in Fig. 11a and c. Here the dipolar interaction was taken into account in (b), but not in (a). The *hfi* coefficients of the removed nuclei are $A_z = [0.01, 0.01]$ MHz and $A^{\pm} = [0.03, 0.01]$ MHz. All other parameters are given in Table 1 with the same $T_{1,n}^{-1}$ for all nuclei. The calculation was performed using the Hilbert space model.

Finally, in Fig. 12 we show the effect of the removal of the core nuclei close to the electron. This narrows the DQ spectra of the remaining nuclei, and results in an increase of their end polarizations. For this calculation two new nuclei further removed from the electron were introduced. Once again, the calculations were done (a) without and (b) with the presence of the nuclear dipolar interaction, and with a constant spin–lattice relaxation rate for all nuclei, $T_{1,n}^{-1} = 0.5\ s^{-1}$. While the dipolar interaction has little effect on the nuclei close to the electron, the polarizations of nuclei removed from the electron, with hardly any *hfi*, depend solely on the dipolar spin diffusion mechanism.

5. Conclusions

The aim of this paper has been to present a renewed perspective of the SE-DNP process using computer simulations based on the spin density matrix representation of the electron–nuclear system while taking relaxation into account. As mentioned in the introduction, previous theoretical treatments of DNP were mostly based on phenomenological rate equations for the bulk polarization. In this work we have shown that important insights can be obtained by considering the full quantum nature of the MW irradiated spin system. The limitation of this type of approach is of course that it can only be applied for small model spin systems, especially when using Liouville space calculations. To enlarge the spin system, we used a Hilbert space approach (reducing the dimension of the calculations from $4^N \times 4^N$ to $2^N \times 2^N$) based on rate equations for the populations of the eigenstates of the spin system. In this way we were able to perform simulations for a system of up to nine-spins with relatively short calculation times (typically minutes), which enabled probing the parameter space affecting the result of the DNP process.

We found that the introduction of a multi-nuclei configuration broadens the frequency range of the SE while reducing its efficiency. This broadening originates from the *hfi* of the nuclei in the core and strongly depends on the core configuration, indicating that dilute core systems can enhance the end polarizations at the edge of the core. Additionally, our calculations indicate that nuclear relaxation gradients can increase the polarizations of the removed nuclei. Above all, they demonstrate the complex dependence of the enhancement mechanism on all relevant parameters of the system.

Only in the last example, we have mentioned the important spin diffusion process that enhances bulk nuclei. This subject will be investigated further in the near future. In an additional publication we will discuss theoretical aspects of the Cross Effect and demonstrate the interaction and relaxation dependence of its efficiency to polarize core nuclei by showing numerical results.

Acknowledgements

We thank Dr. Rangeet Bhattacharyya for his contribution at the early stages of this work. S.V. holds the Joseph and Marian Robbins Chair in Chemical Physics. This research is made in part possible by the historic generosity of the Harold Perlman Family.

Appendix A. Ideal polarization transfer in a multi-nuclear core

To demonstrate the potential of the SE-DNP to enhance all the nuclear spins we consider a system of a single electron *hfi* coupled to N_c core nuclei, where the dipolar interaction between them is neglected. We consider an ideal situation, in which the MW irradiation can excite and saturate all DQ transitions in the system and $T_{1,e}^{-1} \gg T_{1n,DQ,ZQ}^{-1}$ for all transitions. All states $|\beta_e,(M-1)_m^*\rangle$ are connected via the effective MW irradiation to at least one other state of the form $|\alpha_e, M_{m'}^*\rangle$. Then the combination of the ideal DQ MW irradiation together with a $T_{1,e}^{-1}$ relaxation rate brings the populations for all m and m' states to a steady state value according to:

$$p_{\beta_e,(M-1)_m^*}(t) = p_{\alpha_e,M_{m'}^*}(t), \tag{A1}$$
$$\frac{p_{\alpha_e,M_m^*}(t)}{p_{\beta_e,M_m^*}(t)} = \varepsilon_e,$$

which in turn leads to:

$$\varepsilon_e p_{\beta_e,M_m^*}(t) = p_{\alpha_e,M_m^*}(t) = p_{\beta_e,(M-1)_{m'}^*}(t) = \varepsilon_e^{-1} p_{\alpha_e,(M-1)_{m'}^*}(t). \tag{A2}$$

To simplify this derivation we neglected the thermal equilibrium nuclear polarization, $\varepsilon_n = 1$. Starting with the populations of the single states $|\alpha_e,(N_c/2)^*\rangle$ and $|\beta_e,(N_c/2)^*\rangle$ the other populations become for all m:

$$p_{\alpha_e,M_m^*}(t) = \varepsilon^{N_c/2-M} p_{\alpha_e,(N_c/2)^*}$$
$$p_{\beta_e,M_m^*}(t) = \varepsilon^{N_c/2-M} p_{\beta_e,(N_c/2)^*} \tag{A3}$$

The number of states for each M manifold is given by the binomial coefficient $n_M = \binom{N_c}{M+N_c/2}$, and the total population of all states is:

$$Q = \sum_M n_m \varepsilon_e^{N_c/2-M}(1+\varepsilon_e) p_{\beta_e,(N_c/2)^*}(t). \tag{A4}$$

Normalization by setting $Q = 1$ determines the value of $p_{\beta_e,(N_c/2)^*}$:

$$p_{\beta_e,(N_c/2)^*}(t) = (1+\varepsilon_e)^{-(N_c+1)}. \tag{A5}$$

At this point we can evaluate the polarizations of all nuclei. The polarization of the ith nucleus is calculated using all 2^{N_c-1} population differences of the form $(p_{\beta_e,\alpha_i^*,M_m'^*} + p_{\alpha_e,\alpha_i^*,M_m'^*} - p_{\beta_e,\beta_i^*,M_m'^*} - p_{\alpha_e,\beta_i^*,M_m'^*})$, where each of the $M' = -(N_c/2-1/2),\ldots,(N_c/2-1/2)$ states of all $j \neq i$ nuclei has $n'_M = \binom{(N_c-1)}{M'+(N_c-1)/2}$ different M'^*_m values. Using Eq. (A3), the end polarization of this nucleus becomes

$$P_1(t) = \frac{1}{2} Q^{-1} \sum_{M'^*} n'_M \varepsilon_e^{(N_c-1)/2-M'}(1+\varepsilon_e)(1-\varepsilon_e) p_{\beta_e,\alpha_e,(N_c/2-1/2)^*}. \tag{A6}$$

Combining this with Eqs. (A4) and (A5) results in an end polarization of

$$P_i(t) = \frac{1}{2}\frac{1-\varepsilon_e}{1+\varepsilon_e} \tag{A7}$$

for all nuclei i. This is exactly equal to the electron polarization at $t = 0$. This ideal case can of course also be considered for ZQ irradiation, and will result in end polarizations of all nuclei that are equal to $-P_e(0)$.

References

[1] D. Hall, D. Maus, G. Gerfen, S. Inati, L. Becerra, F. Dahlquist, R. Griffin, Science 276 (1997) 930–932.
[2] M. Rosay, J. Lansing, K. Haddad, W. Bachovchin, J. Herzfeld, R. Temkin, R. Griffin, J. Am. Chem. Soc. 125 (2003) 13626–13627.
[3] R. Nelson, M. Sawaya, M. Balbirnie, A. Madsen, C. Riekel, R. Grothe, D. Eisenberg, Nature (London) 435 (2005) 773–778.
[4] J. Ardenkjr–Larsen, B. Fridlund, A. Gram, G. Hansson, L. Hansson, M. Lerche, R. Servin, M. Thaning, K. Golman, Proc. Natl. Acad. Sci. USA 100 (2003) 10158–10163.
[5] M.E. Merritt, C. Harrison, C. Storey, F.M. Jeffrey, A.D. Sherry, C.R. Malloy, Proc. Natl. Acad. Sci. 104 (2007) 19773–19777.
[6] A.W. Overhauser, Phys. Rev. 92 (1956) 411–415.
[7] T.R. Carver, C.P. Slichter, Phys. Rev. 92 (1953) 212–213.
[8] T.R. Carver, C.P. Slichter, Phys. Rev. 102 (1956) 975–980.
[9] L.H. Bennett, H.C. Torrey, Phys. Rev. 108 (1957) 499–500.
[10] K.H. Hausser, D. Stehlik, Conc. Magn. Reson. 3 (1968) 79–139.
[11] W. Mueller-Warmuth, K. Meise-Gresch, Adv. Magn. Reson. 11 (1983) 1–45.
[12] C. Jefferies, Phys. Rev. 106 (1957) 164–165.
[13] A. Abragam, W.G. Proctor, CR Hebd. Seances Acad. Sci. 246 (1958) 2253–2256.
[14] T.J. Schmugge, C.D. Jeffries, Phys. Rev. 138 (1965) A1785–A1801.

[15] C.D. Jeffries, Dynamic Nuclear Orientation, John Wiley, New York, 1963.
[16] M. Borghini, A. Abragam, CR Hebd. Seances Acad. Sci. 203 (1959) 1803.
[17] O. Leifson, C.D. Jeffries, Phys. Rev. 1122 (1961) 1781.
[18] A. Abragam, M. Goldman, Nuclear Magnetism: Order and Disorder, Clarendon, Oxford, 1982.
[19] A. Abragam, M. Goldman, Rep. Prog. Phys. 41 (1978) 395–467.
[20] R.A. Wind, M.J. Duijevestijn, C. Van Der Lugt, A. Manenschijn, J. Vriend, Prog. NMR Spectrosc. 17 (1985) 33–67.
[21] A. Abragam, M. Borghini, Progress in Low Temperature Physics, vol. 4, North-Holland, Amsterdam, 1964.
[22] A.G. Redfield, Phys. Rev. 98 (1955) 1787–1809.
[23] I. Solomon, in: J. Smidt (Ed.), Magnetic and Electric Resonance and Relaxation North-Holland, Amsterdam, 1963.
[24] B.N. Provotorov, Soviet Phys. JETP 14 (1962) 1126.
[25] C.F. Hwang, D.A. Hill, Phys. Rev. Lett. 18 (1967) 110–112.
[26] A.V. Kessenikh, V.I. Lushchikov, A.A. Manenkov, Y.V. Taran, Sov. Phys. Solid State 5 (1963) 321–329.
[27] A.V. Kessenikh, A.A. Manenkov, G.I. Pyatnitskii, Sov. Phys. Solid State 6 (1964) 641–643.
[28] C.F. Hwang, D.A. Hill, Phys. Rev. Lett. 19 (1967) 1011–1013.
[29] D.S. Wollan, Phys. Rev. B 13 (1976) 3671–3685.
[30] C.T. Farrar, D.A. Hall, G.J. Gerfen, J. Chem. Phys. 114 (2001) 4922–4933.
[31] M.J. Duijvestijn, R.A. Wind, J. Smidt Phys. 138B (1986) 147–170.
[32] T. Maly, G.T. Debelouchina, V.S. Bajaj, K.-N. Hu, C.-G. Joo, M.L. Mak-Jurkauskas, J.R. Sirigiri, P.C.A. van der Wel, J. Herzfeld, R.J. Temkin, R.G. Griffin, J. Chem. Phys. 128 (2008) 052211.
[33] V. Denysenkov, M.J. Prandolini, M. Gafurov, D. Sezer, B. Endeward, T.F. Prisner, Phys. Chem. Chem. Phys. 12 (2010) 5786–5790.
[34] E.V. Kryukov, M.E. Newton, K.J. Pike, D.R. Bolton, R.M. Kowalczyk, A.P. Howes, M.E. Smith, R. Dupree, Phys. Chem. Chem. Phys. 12 (2010) 5757–5765.
[35] J.A. Villanueva-Garibay, G. Annino, P.J.M. van Bentum, A.P.M. Kentgens, Phys. Chem. Chem. Phys. 12 (2010) 5846–5849.
[36] L.R. Becerra, G.J. Gerfen, B.F. Bellew, J.A. Bryant, D.A. Hall, S.J. Inati, R.T. Weber, S. Un, T.F. Prisner, A.E. McDermott, K.W. Fishbein, K.E. Kreischer, R.J. Temkin, D.J. Singel, R.G. Griffin, J. Magn. Reson. A 117 (1995) 28–40.
[37] Kan-Nian Hu, Vikram S. Bajaj, Melanie Rosay, Robert G. Griffin, J. Chem. Phys. 126 (2007) 044512.
[38] K.R. Thurber, W. Yau, R. Tycko, J. Magn. Reson. 204 (2010) 303–313.
[39] K. Hu, H. Yu, T. Swager, R. Griffin, J. Am. Chem. Soc. 126 (2004) 10844.
[40] A. Schweiger, G. Jeschke, Principles of Pulse Electron Paramagnetic Resonance, Oxford University Press, New York, 2001.
[41] C. Ramanathan, Appl. Magn. Reson. 34 (2008) 409–421.
[43] R.R. Ernst, G. Bodenhausen, A. Wokaun, Principles of Nuclear Magnetic Resonance in One and Two Dimensions, Oxford University press, New York, 1987.
[44] C.P. Slichter, Principles of Magnetic Resonance, Springer, Berlin Heidelberg, 1990.
[45] V. Nagarajan, Y. Hovav, A. Feintuch, S. Vega, D. Goldfarb, J. Chem. Phys. 132 (2010) 214504.
[46] M. Eden, M.H. Levitt, J. Magn. Reson. 132 (1998) 220–239.
[47] B. Stevensson, M. Eden, J. Magn. Reson. 181 (2006) 162–176.

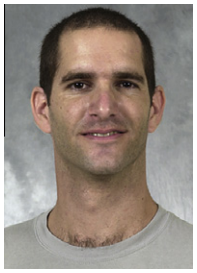

Yonatan Hovav is a Ph.D. student in the group of Professor Shimon Vega, at the Chemical Physics department, Weizmann Institute of Science, Israel. He received his B.Sc. degree in biotechnology-engineering from Ben Gurion University in Israel. His M.Sc. research work, performed in the laboratory of Prof. Shimon Vega, was in the field of solid state NMR and Para Hydrogen Induced Polarization. During his Ph.D. studies he explores new theoretical and experimental aspects in the field of DNP on diamagnetic samples in the solid state.

Akiva Feintuch is a Staff Scientist at the department of Chemical Physics in the Weizmann Institute of Science in Israel. He received his Ph.D. at the Racah Institute of Physics at the Hebrew University in Jerusalem under the supervision of Professor Noam Kaplan. His postdoctoral work was conducted at the Mouse Imaging Centre, Hospital for Sick Kids in Toronto with Professor Mark Henkelman. His present research interests include theoretical and experimental aspects of Dynamic Nuclear Polarization.

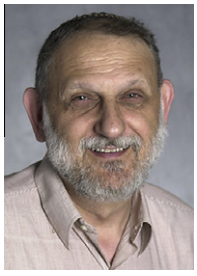

Shimon Vega is a professor at the Department of Chemical Physics at the Weizmann Institute of Science in Israel. He received his Ph.D. at the Weizmann Institute under the supervision of Prof. Zeev Luz. His postdoctoral research was performed at the University of California, Berkeley, with Professor Alex Pines. His present research interests include solid state NMR, dynamic MAS NMR and theoretical and experimental aspects of Dynamic Nuclear Polarization.